A Reversible Hydrogen Ion Battery

A thesis submitted towards partial fulfillment of
BS-MS Dual Degree Programme

By

Neethu C D
(BS-MS student, Registration No.: 20121014)

Under the guidance of,

Dr. Muhammed Musthafa O T,

Assistant Professor,

Department of Chemistry
Indian Institute of Science Education and Research (IISER)
Pune, India

Certificate

This is to certify that this dissertation entitled **"A Reversible Hydrogen Ion Battery"** towards the partial fulfillment of the BS-MS dual degree programme at the Indian Institute of Science Education and Research Pune, represents original research carried out by **Neethu C D** at IISER Pune Under the supervision of **Dr. Muhammed Musthafa O T, Assistant Professor, Department of Chemistry, IISER Pune** during the academic year of 2016-2017.

Date: 31/03/17

Place: Pune

Dr. Muhammed Musthafa O T

Assistant Professor

Department of Chemistry

IISER Pune

डॉ.मुहमद मुस्तफा/ Dr. Muhammed Musthafa
सहायक प्राध्यापक/ Assistant Professor
भारतीय विज्ञान शिक्षा एवं अनुसंधान संस्थान
Indian Institute of Science Education & Research
पुणे-411 008, भारत/ Pune - 411 008, India

Declaration

I hereby declare that the matter embodied in the report entitled **"A Reversible Hydrogen Ion Battery"** are the results of the investigations carried out by me at the Department of Chemistry, IISER Pune, Under the supervision of Dr. **Muhammed Musthafa O.T, Assistant Professor, Department of Chemistry, IISER, Pune** and the same has not been submitted elsewhere for any other degree.

Neethu C D

Date: 31/03/17

Place: Pune

Acknowledgement

It is a pleasure to express my deep sense of thanks and gratitude to my mentor and guide **Dr.Muhammed Musthafa O. T., Assistant Professor, Department of Chemistry IISER Pune.** His continuous support and keen interest above all his overwhelming attitude to help to his students had been solely and mainly responsible for completing my work.

I would like to express my gratitude to **Dr. P. A. Joy, Chair, Physical and Materials Chemistry Division, NCL Pune** for his continuous support throughout my project.

I owe a deep sense of gratitude to **Dr. Ravikumar** for his timely advice, scientific approach and helping me with the understandings of electrochemical techniques.

It is my privilege to thank **Zahid Bhat, Mruthyunjayachari, Alagar Raja, Mohammed Fawaz, Manu Gautam** and all my lab mates for their kind help and co-operation throughout my research work.

I sincerely thank **Dr. Pramod Pillai** and **Dr. Shivprasad Patil** for giving me consent to use the UV-Vis and Raman instruments. I would like to thank **Soumendu Roy** and **Ajith V J** for being a helping hand during data collection.

I am extremely thankful to my family members for their constant encouragement and moral support throughout my research period.

Last but not the least thanks to Indian Institute of Science Education and research, Pune for providing outstanding and sublime research facilities.

List of tables

No	Title	Page no
2.1	Instruments used	22
3.1	Electrochemical parameters extracted from RRDE experiments	32
3.2	Electrochemical parameters extracted from RDE experiments	32

List of illustrations

No	Title	Page no
1.1	(a) Schematic representation of effect of global warming on our environment, (b)-(d) Effects of global warming on the flora and fauna thriving on this planet	10
1.2	(a) UN conference on climate change and (b) logo of Paris conference	11
1.3	Schematic representation of the working principle behind a solar cell	12
1.4	Schematic illustration of (a) double layer capacitor (b) pseudo capacitor	12
1.5	Schematic representation of battery discharging	13
1.6	(a) Photograph of Sir William Grove (b) illustration of his gas battery	14
1.7	(a) Schematic representation of fuel cell (b) its role in sustainable energy chain	15
1.8	Schematic representation of chemically chargeable battery	17
1.9	Schematic representation of electrically chargeable battery	18
2.1	Photograph of graphite plates with parallel flow fields	21
2.2	(a) The applied voltage on working electrode with respect to time and (b) the current response of this applied voltage	23
2.3	(a) RDE linear sweep voltammogram profile for oxidation, (b) Levich plot, (c) Koutecky-levich plot	24

2.4	Schematic representation of Attenuated Total Reflectance (ATR) IR Spectroscopy	27
2.5	(a) Basic principles of Raman analyser. (b) Possible scattering radiations	27
3.1	Schematic representation of chemically chargeable battery.	29
3.2	(a) Cyclic voltammogram of benzoquinone (Q) in 0.5 M H_2SO_4 on a glassy carbon electrode at different scan rates (b) pH vs. potential (Pourbiax diagram) (c) Plot of peak current vs. square root of scan rate during the oxidation scan (d) the corresponding log (i) vs. log (υ) plot.	30
3.3	Cottrel plot I vs. reciprocal of square root time (a) for hydroquinone and (b) benzoquinone.	31
3.4	Single electrode potentials of Q and QH_2 electrode with respect to H_2/H^+ and O_2/H_2O half-cell reactions	31
3.5	(a) RRDE of QH_2 oxidation and reduction at a scan rate of 10 mV/s (b) RDE of QH_2 oxidation (c) RDE of Q reduction (d) Kouteckey-Levich plots for QH_2 oxidation (e) Kouteckey-Levich plots for Q reduction.	33
3.6	In-situ UV-Vis spectroelectrochmistry data for the redox reaction of quinone. (a) Cyclic voltammogram at a scan rate of 5 mV/s. (b) the potential dependent spectra acquired during the oxidation scan and (c) during the reduction scan.	34
3.7	Scheme of air chargeable and reversible H^+ ion battery with possible electrode reactions	36
3.8	(a) In-situ solid state cyclic voltammogram, (b) Galvanosatatic Intermittent Titration Technique	37
3.9	Polarization curves for (a) H_2-Q battery and (b) O_2-QH_2 battery (c) Galvanostatic polarization curves for H_2-Q (10 mA/cm^2) and O_2-QH_2 (5 mA/cm^2) batteries (d) Extended cyclability of H_2-Q at 10 mA/cm^2 and (e) O_2-QH_2 batteries at 5 mA/cm^2	38

3.10	UV-Vis spectra of (a) H_2-Q battery cathode and (b) O_2-QH_2 battery anode during different discharge cycles. FTIR spectra of (c) H_2-Q battery cathode and (d) O_2-QH_2 battery anode during different discharge cycles. Raman spectra of (e) H_2-Q battery cathode and (f) O_2-QH_2 battery anode during different discharge cycles.	40
3.11	Molecular structure of Quinone (Q), Hydroquinone (QH_2) and Quinhydrone	41
3.12	(a) Galvanostatic charge discharge curves at different rates for H_2-Q battery (b) Cell voltage vs. rate plot during discharge and charge chemistries. (c) Galvanostatic cycling at a rate of 50 mA/cm^2 for 300 cycles for H_2-Q battery.	42
3.13	UV-Vis spectra of H_2-Q battery cathode (a) during the discharge and (b) during the charge cycle. FTIR spectra of H_2-Q battery cathode (c) during the discharge and (d) during the charge cycles. Raman spectra of H_2-Q battery cathode (e) during the discharge and (f) during the charge cycles.	43

TABLE OF CONTENTS

ABSTRACT 9

CHAPTER 1. INTRODUCTION

1.1 Solar cell 11

1.2 Super capacitor 12

1.3 Battery 13

1.4 Fuel cell 14

CHAPTER 2. MATERIALS & METHODS

2.1 Chemicals used 19

2.2 Experimental section 19

2.2.1 Battery fabrication 21

2.3 Techniques

2.3.1 Electrochemical techniques

2.3.1.1 Cyclic voltammetry 22

2.3.1.2 Rotating disc electrode (RDE) technique 24

2.3.1.3 Rotating ring disc electrode (RRDE) technique 26

2.3.2 UV-Vis spectroscopy 26

2.3.3 Attenuated Total Reflectance (ATR) FT-IR Spectroscopy 26

2.3.4 Raman spectroscopy 27

CHAPTER 3. RESULTS & DISCUSSION

3.1 Introduction 29

3.2 Chemically chargeable and reversible H^+ ion battery 29

3.3 Electrically chargeable H^+ ion battery 41

CHAPTER 4. CONCLUSIONS 44

REFERENCES 45

ABSTRACT

We demonstrate the proof of concept of an air chargeable and reversible H^+-ion battery by exploiting the catalytic nature of Pt@C electrocatalyst in ionizing H_2 and O_2 molecules and the proton coupled and reversible redox energy transformation between quinone (Q) and hydroquinone (QH_2) molecules. The unique feature of this battery is such that it delivers output power during discharge and air charge process making it a reversible H^+-ion battery. Such a battery could be cycled for 200 cycles with decent capacity retention with concomitant power production during the discharge and air charge chemistries. Electrochemistry, Galvano-static intermittent titration technique (GITT), rotating ring disk electrode (RRDE) measurements, UV-Vis spectroelectrochemistry, FTIR and Raman spectroscopic analysis reveal a transition from Q to QH_2 during the discharge chemistry. However during the air charge chemistry, formation of quinhydrone, the charge transfer complex between quinone and hydroquinone was dominantly observed. The catalytic nature of Pt@C towards H_2 oxidation could be further exploited to design an electrically rechargeable H^+-ion battery which could be cycled for over 300 cycles with decent capacity retention. Investigation by various physico chemical techniques revealed a reversible redox energy transition between Q and QH_2 (possibly via quinhydrone) during discharge and electrical charge processes. In an era of energy crisis, it is indeed inevitable to store and use every bit of energy and we believe our strategy is a right step ahead in this direction.

CHAPTER 1. INTRODUCTION

Energy plays an important role in every-day life. Being in this technologically advancing era energy plays an inevitable part[1, 2]. For the sustainable growth we need energy from sources which are compatible with the environment[4, 5]. But compared to the availability of renewable sources only a few of it's been efficiently used. The rest of the energy is produced from non-renewable sources, mostly fossil fuels[5]. Combustion of fossil fuel results in emission of various poisonous gases and huge lot of CO_2[6], the greenhouse gas which plays a huge role in global warming[7, 8]. Global warming have markedly effected the polar ice to melt. Melting rates have strike alarming value of 3% per decade. Its effect also include climatic changes, sea level rising, coral reef bleaching, food chain breakage, health issues etc[6].

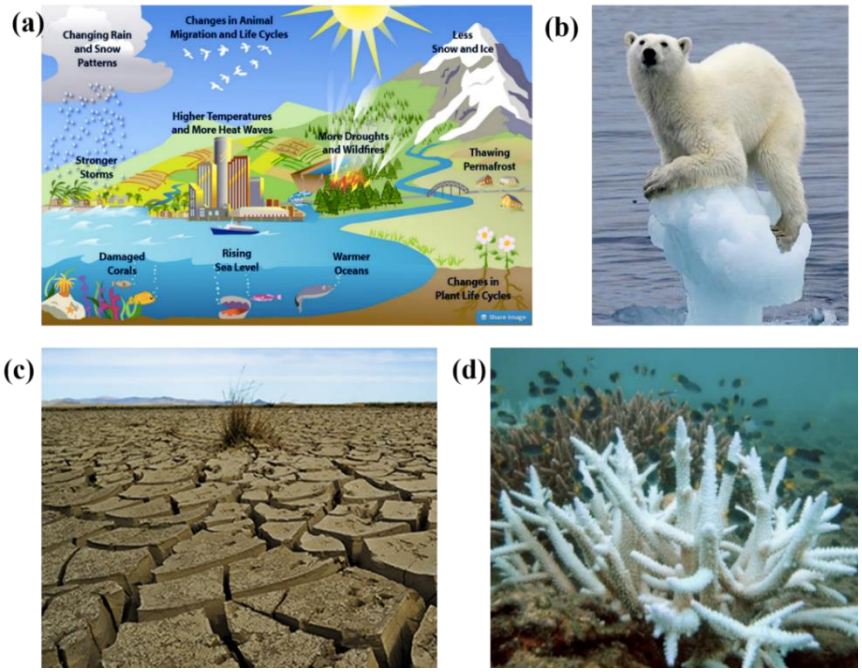

Figure 1.1: (a) Schematic representation of effect of global warming on our environment *(http://planetsave.com/2015/06/02/global-warming-or-climate-change-whats-the-difference/S)*. (b) - (d) Effects of global warming on the flora and fauna thriving on this planet (*https://sites.google.com/a/d303.org/harry--endangered-polar-bears/global-warming-and-climate-change),(https://www.uea.ac.uk/about/-/climate-change-pledges-could-avoid-significant-effects-of-global-warming), (https://en.wikipedia.org/wiki/Coral_bleaching#/media/File:Keppelbleaching.jpg)*

In this context, during the UN conference on climate change, held in Paris on Dec 2015 world leaders have unanimously agreed to limit the global warming temperature to 1.5 ^{o}C *(http://unfccc.int/meetings/paris_nov_2015/meeting/8926.php).* To achieve this target of 1.5 ^{o}C we should focus on developing zero emission technologies at least by 2050.

Figure 1.2: (a) UN conference on climate change and (b) logo of Paris conference. *(http://www.panoramas.pitt.edu/art-and-culture/2-degrees-or-15-what-paris-climate-agreement-means-caribbean)* *(http://unfccc.int/meetings/paris_nov_2015/meeting/8926.php)*

Electrochemical energy storage and conversion devices such as fuel cell, batteries, supercapacitors and solar cells are potential zero emission technologies as noted below.

1.1 SOLAR CELL

Solar cell are energy conversion device that can convert light energy into electrical energy. Different type of solar cell are available depending on the materials used. Most widely used ones are based on silicon, P- N junction diode. Sunlight consist of photons, tiny particle of particular energy. As the light fall on N type semi-conductor, it knocks out an electron (negative charge) leaving a hole (positive charge). Due do the electric field at the P- N junction electron cannot cross to N-type semiconductor from P-type but hole can.

Electron travels through external circuit powering a load or charging a battery and reach the P-type semiconductor[9].

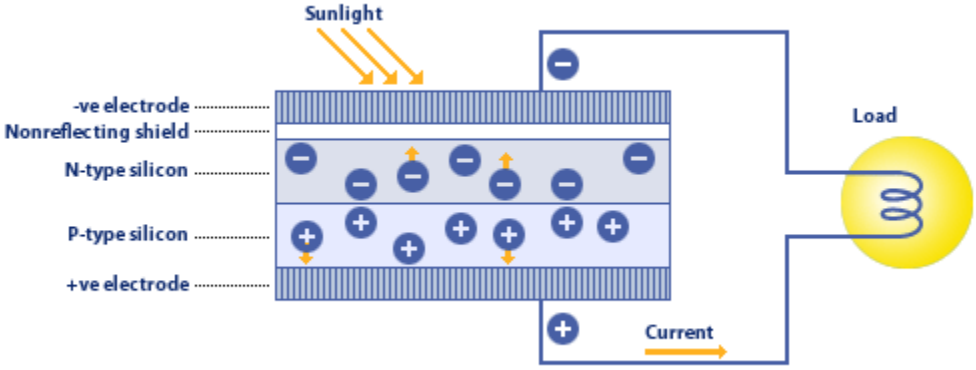

Figure 1.3: Schematic representation of the working principle behind a solar cell. *(http://www.mitsubishielectric.com/bu/ solar/faq/index.html)*

1.2 SUPERCAPACITOR

Supercapacitors are well known for their rapid charging and discharging ability. They consists of two electrode with huge area in electrolyte separated via a separator.

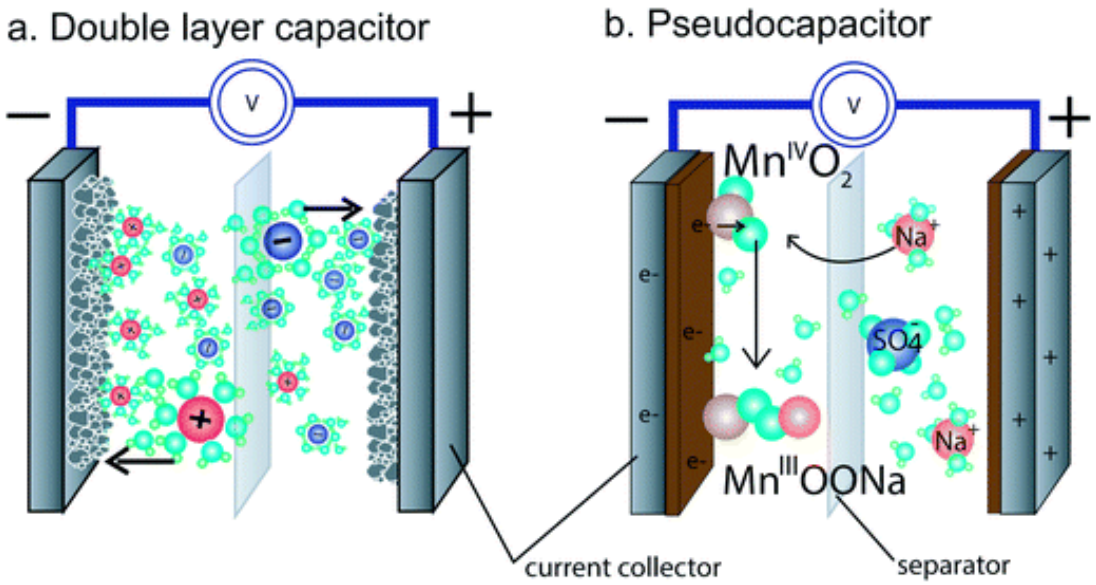

Figure 1.4: Schematic illustration of (a) double layer capacitor and (b) pseudo capacitor (*J. Mater. Chem. A, 2014, 2, 10776*)

There are mainly two kind of electrochemical capacitors electric double layer capacitors and pseudo capacitors. On charging the electrodes, opposite charges develop on either sides of the separator creating electric double layer of nanometer thickness which is non-faradic in nature in the case of double capacitors. This is why it's been called as double layer capacitors as well as electric double layer capacitor (EDLCs) [10]. Pseudo capacitors undergo charge and discharge via fast redox reaction on the electrode surfaces[11].

1.3 BATTERY

Batteries are self-contained units[10], which produces electrical energy by converting the stored chemical energy, which can be used for powering various appliances. There are mainly 2 type of batteries. Primary batteries which can be discharged as long as chemicals available and then discarded. Examples include, Al-air, Zn-C and Daniel cell. Secondary batteries which can be discharged as primary batteries. However the process of discharging can be reversed by applying a current in the opposite direction[12].

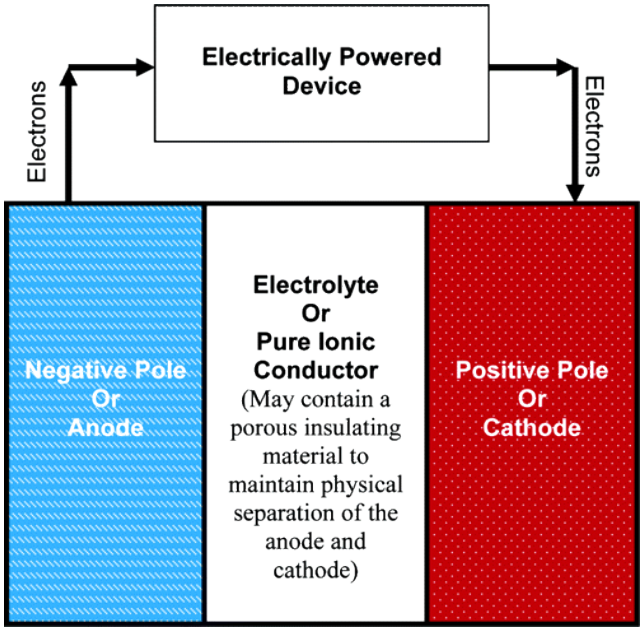

Figure 1.5: Schematic representation of battery discharging *(Chem. Rev. 2004, 104, 4245-4269*)

Battery architecture consists of two electrodes, anode where oxidation happens and cathode where reduction happens, physically separated by electrolyte or purely ionic

conductor. Figure 1.5 shows battery being discharged with an external load. If battery is recharging, instead of external load, a power source will be connected across the electrodes, which will reverse the direction of electron flow thus reaction will be reversed. This will make the battery ready for the next burst of power. Typical secondary batteries are Pb-acid, metal-ion and metal hydride batteries.

Even though batteries and super capacitors are considered as zero emission technology, manufacturing of their architectural components involve considerable amounts of CO_2 emission, which will not be insignificant in a foreseeable future. For this reason, fuel cell is the true zero emission technology as explained below.

1.4 FUEL CELL

Fuel cell was invented by William Grove in 1843, what he called as gas battery[13]. He used similar metal platinum on both electrode, unlike the battery architecture present those days. But filled one compartment with H_2 gas and the other with O_2 gas and observed a potential of 0.6 V.

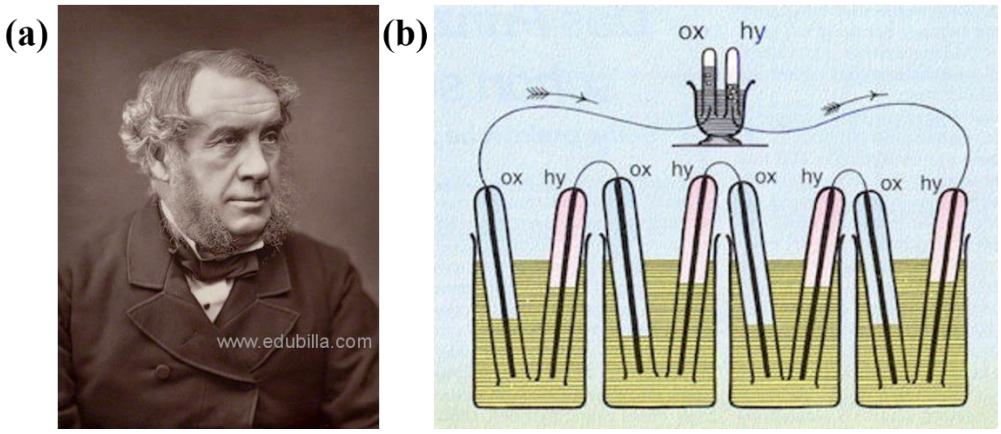

Figure 1.6: (a) Photograph of Sir William Grove (b) Illustration of his gas battery. ***(http://www.edubilla.com/inventor/william-robert-grove/), (http://home.uni-leipzig.de/energy/ef/14.htm)***

He further added many such cell in series to increase in potential. This output was then connected again to two platinum electrodes immersed in water resulting in evolution of H_2 and O_2 gases at respective electrodes. Thus he proved that if by combining H_2 and O_2 gases electricity can be produced then, by applying electricity this can be reversed.

But this did not gain much attention until 1969, when NASA used this technology in Apollo mission to land on moon[14]. This provided double benefit for astronauts as combining H_2 and O_2 provide energy as well as a source of drinking water.

Most popularly known and the simplest one is Polymer Electrolyte Membrane Fuel Cell (PEMFC) [15]. PEMFC uses hydrogen and oxygen as fuels therefore it is also called H_2-O_2 fuel cell. Both anodes and cathodes are made up of Pt@C as platinum is benchmark catalyst for oxygen reduction reaction[15-17] as well as hydrogen oxidation reaction[18]. Respective compartments are separated by a proton conducting Nafion® membrane. Hydrogen gets oxidised at anode to hydrogen ions and electrons (equation 1). At cathode oxygen get reduced by accepting protons (that migrate through Nafion®) and electrons (travelling through external circuit powering the load) and produce water (equation 2). On providing pure hydrogen fuel cell produce only heat and water as the by product. Therefore it is a true zero emission technology.

Anodic reaction	**$2H_2$**	**→**	**$4H^+ + 4e^-$**	**…… (1)**
Cathodic reaction	**$O_2 + 4H^+ + 4e^-$**	**→**	**$2H_2O$**	**…… (2)**
Net cell reaction	**$2H_2 + O_2$**	**→**	**$2H_2O$**	**…… (3)**

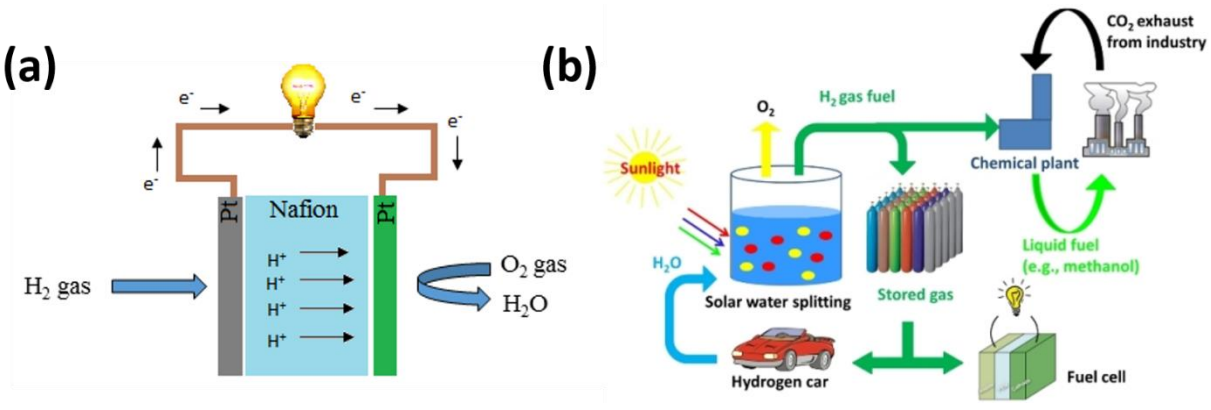

Figure 1.7: (a) Schematic representation of fuel cell and (b) its role in sustainable energy chain. *(http://chethoughts.com/solar-water-splitting-a-step-towards-carbon-free-energy-and-environment/)*

Fuel cell have the ability to produce electricity as well as water (equation 3) by combining H_2 and O_2. If water can be split to H_2 and O_2 in a process called artificial photosynthesis it represents a means of storing the energy of the sun in the chemical bonds of fuel molecules[19]. It is critically important given the geographic and temporal variations of renewable energy sources. The stored fuel molecules can be transported to areas where it can be combined in a fuel cell to produce electricity. The byproduct of this reaction is again water. Figure (b) shows good model in using solar energy to produce fuels, which can be fed to a fuel cell to produce energy in a sustainable way. For this reason fuel cell occupies the heart of sustainable energy chain.

Even though fuel cell provide clean energy[20], its commercial out-reach is hindered by its cost of electricity production per kW. The commercial inaccessibility is mainly due to the expensive proton shuttling membrane (Nafion®) and expensive Pt based electro catalyst[16, 21, 22]. 80% of efficiency losses in a fuel cell arises due to the positive electrode, therefore the cathode requires the heaviest precious metal loading[16, 22]. If fuel cell technologies are ever to succeed as potential zero emission technologies, it is indeed inevitable to reduce the cost of these architectural components to a level of commercial accessibility.

Here we show a diverse strategy for developing a reversible and air chargeable H^+-ion battery by altering the interfacial chemistry at the cathode (precious metal based) of the state of the art fuel cell by a molecular species (Quinone) supported on carbon nanoparticles that can undergo fast proton coupled electron transfer reversibly, Scheme 1. This lead to a hydrogen based energy device without any precious metals on the cathode side. It consist of 2 electrodes, Pt@C electrode as electrode 1 and benzoquinone@C (Q@C) as electrode 2 which are separated by proton conducting Nafion® membrane, scheme 1. On filling hydrogen on Pt@C electrode compartment, as Pt being popular electrocatalyst for hydrogen oxidation, H^+-ions and electrons are produced at electrode 1(equation 4). This H^+-ions reach Q@C electrode via Nafion® membrane and electrons via external circuit, by powering an external load. At Q@C electrode, benzoquinone (Q) get reduced to hydroquinone (QH_2) by accepting H^+-ions and electrons (equation 5). When Pt@C is acting as anode (oxidation) and Q@C is acting

as cathode (reduction), the resulting battery can be termed as battery forward (BF) or H_2-Q battery.

After the discharge of H_2-Q battery if electrode 1 compartment is supplied with oxygen, a species with positive redox energy, QH_2@C undergoes oxidation to Q by releasing H^+-ions as well as electrons (equation 6 and 7). H^+-ion reach electrode 1 via Nafion® and electrons via external circuit, again powering an external load. QH_2@C act as anode (oxidation) and O_2 on Pt@C act as cathode (reduction) and this battery can be termed as battery reverse (BR) or O_2-QH_2 battery. Battery reverse configuration is similar to a fuel cell as oxygen get reduced by accepting H^+-ions and electrons producing water. It should be noted that Pt@C is a very good catalyst for oxygen reduction reaction as well [15-17]. Most importantly O_2-QH_2 battery discharge make the H_2-Q battery ready for the next burst of power and vice versa. Since Pt@C is a good catalyst for H^+-ion reduction as well[18, 23], this concept further leads to an electrically rechargeable H^+-ion battery, scheme 2 and equations 8 and 9.

As BF and BR assist each other with power outputs, we denote the term a reversible and air chargeable H^+-ion battery to denote the same.

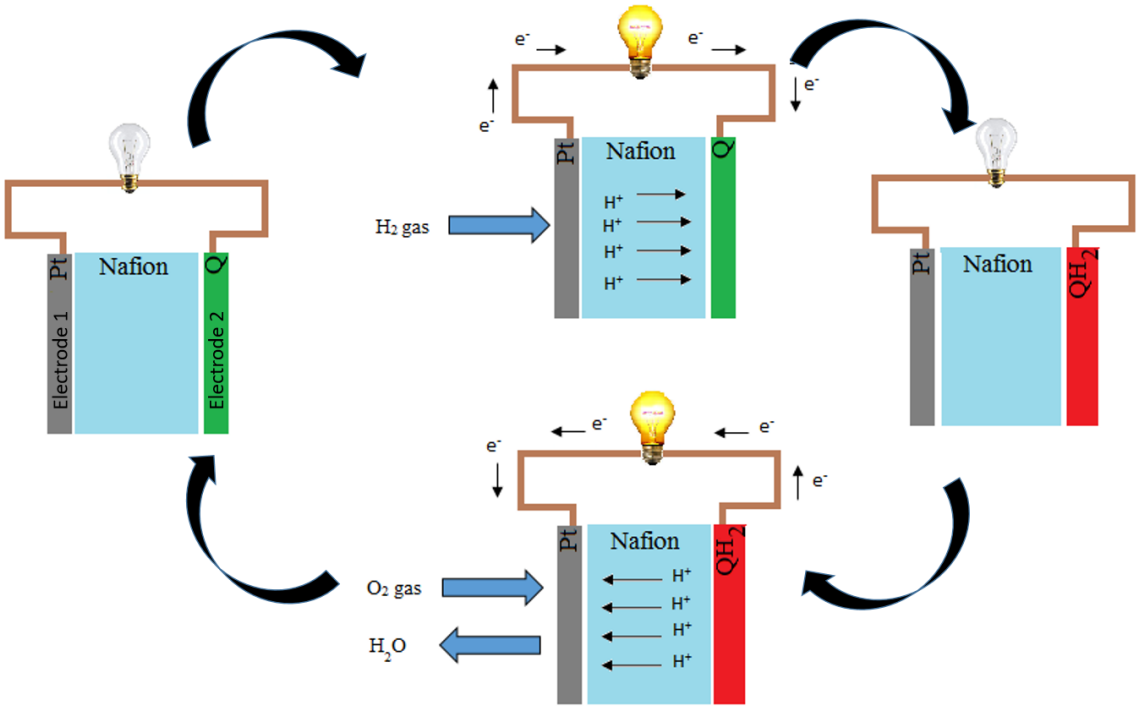

Figure 1.8: Schematic representation of chemically chargeable battery

On passing Hydrogen

Pt@C electrode (anode) $H_2 \rightarrow 2H^+ + 2e^-$ …… (4)

Quinone electrode (cathode) $Q + 2H^+ + 2e^- \rightarrow QH_2$ …… (5)

On passing Oxygen

Quinone electrode (anode) $QH_2 \rightarrow Q + 2H^+ + 2e^-$…… (6)

Pt@C electrode (cathode) $\frac{1}{2}O_2 + 2H^+ + 2e^- \rightarrow H_2O$ …… (7)

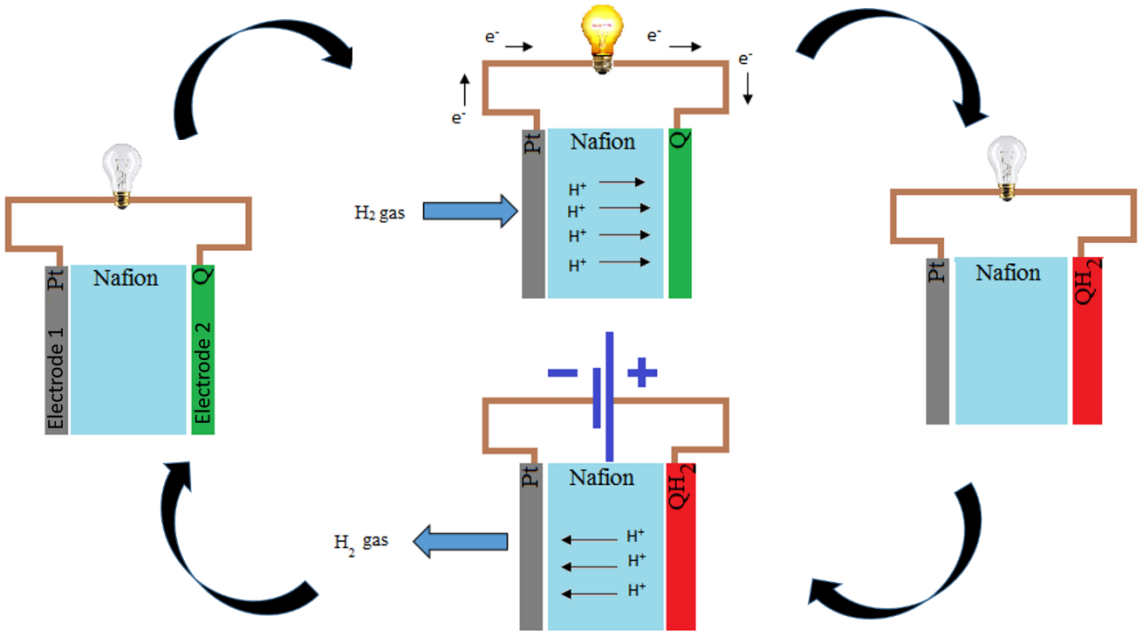

Figure 1.9: Schematic representation of electrically chargeable battery

On Charging

Quinone electrode (anode) $QH_2 \rightarrow Q + 2H^+ + 2e^-$…… (8)

Pt@C Electrode (cathode) $2H^+ + 2e^- \rightarrow H_2$ …… (9)

The unique aspect of this battery is such that it produces a power output during the discharge as well chemical charge process making it a reversible and chemically chargeable H^+-ion battery. In an era of energy crisis it is inevitable to store and utilize every bit of energy available and we believe our strategy is a right step ahead in this direction.

CHAPTER 2. MATERIALS & METHODS

2.1 CHEMICALS

1,4-Benzoquinone $C_6H_4O_2$ (Alfa Aesar), 1,4-Hydroquinone $C_6H_4(OH)_2$ (SDFCL), Quinhydrone $C_{12}H_{10}O_4$ (Alfa Aesar), Nafion® $C_7HF_{13}O_5S \cdot C_2F_4$ (5 wt% in lower aliphatic alcohols and water) (Aldrich), Isopropyl alcohol(IPA) (C_3H_8O), carbon powder(super P, Vulcan carbon), Platinum 40 wt% carbon powder, Citric acid $C_6H_8O_7$ (Alfa Aesar), Trisodium citrate $C_6H_5O_7Na_3$ (SDFCL) , Monopotassium phosphate KH_2PO_4 (Alfa Aesar), Dipotassium phosphate K_2HPO_4 (Alfa Aesar), Borax $Na_2B_4O_7 \bullet 10H_2O$ (Rankem), Sodium hydroxide NaOH (SDFCL).

2.2 EXPERIMENTAL SECTION

Cyclic voltammograms were collected in nitrogen atmosphere at different scan rates 5, 10, 15, 20, 25, 30, 40, 50 mV/s, in three electrode system with glassy carbon (GC) as working electrode, Ag/AgCl (3 M KCl) as reference electrode, platinum wire as counter in 10 mM benzoquinone solution in 0.5 M H_2SO_4. pH dependent behavior of benzoquinone was exploited with cyclic voltammogram of 10 mM of benzoquinone in different pH buffer solutions like citrate buffer (pH = 4, 5), phosphate buffer (pH = 6, 7), borate buffer (pH = 9, 10) at different scan rates in nitrogen atmosphere and 3 electrode system as mentioned above.

Single electrode potential was found in nitrogen atmosphere using two electrode system with GC as working electrode and Ag/AgCl (3 M KCl) as reference electrode in 5 mM benzoquinone solution in 0.5 M H_2SO_4 and 5 mM hydroquinone solution in 0.5 M H_2SO_4.

RRDE was done with nitrogen purged solution of 1 mM hydroquinone in 0.5 M H_2SO_4 at a scan rate of 10 mV/s with three electrode system containing platinum disc-platinum ring (Pt-Pt) electrode as working electrode, Ag/AgCl (3 M KCl) as reference electrode, platinum wire as counter at different RPM values (100, 400, 900, 1600, 3600). RDE was done with solutions of hydroquinone and benzoquinone of 1 mM concentration in the same conditions as used above.

Simultaneous spectro-electrochemistry data of quinone-hydroquinone was collected with 1 mM hydroquinone in 0.5 M H_2SO_4 at a scan rate of 5 mV/s with three electrode system with platinum mesh electrode as working electrode, Ag/AgCl (3 M KCl) as reference electrode, platinum wire as counter electrode. The spectrum of hydroquinone was taken as the background, therefore negative absorption peak indicate its depletion.

Solid state CV analysis Q@C electrodes where made by coating ink containing Q powder, super P powder, 10 wt % Nafion® in isopropyl alcohol (IPA) on toray carbon sheet (2x2 cm^2 dimension). Properly dried electrodes were assembled in fuel cell set up with Pt@C as electrode 1 and Q@C as electrode 2 separated by pre-treated Nafion® membrane. Electrode 2 was always kept under nitrogen (N_2) atmosphere to avoid contact with any other gas. All CVs were collected at a scan rate of 5 mV/s. Blank profile was collected by passing N_2 on both electrodes with Q@C electrode as WE. Profile for H_2-Q battery was collected by passing H_2 on Pt@C electrode with Q@C electrode as WE. Profile for O_2-QH_2 battery was collected by passing O_2 on Pt@C electrode with QH_2@C electrode as WE.

For GITT analysis Q@C electrodes preparations and setup was similar as for the solid state CV analysis. Electrode 2 was always kept under nitrogen (N_2) atmosphere to avoid contact to any other gas. Electrode 2 compartment was filled with H_2 and discharge was done for 5 minutes with 250 µA current followed by one hour relaxation time and the process was repeated for several hours.

For Polarization and charge discharge data collection, Q@C electrodes preparations and setup was similar as for the solid state CV analysis and GITT. Electrode 2 was always kept under nitrogen (N_2) atmosphere to avoid contact to any other gas. Depending on mode of operation, the H_2 or O_2 were supplied to the electrode 1 chamber.

Q@C electrodes preparations and setup was similar as for the solid state CV analysis and GITT. Electrode 2 was always kept under nitrogen (N_2) atmosphere to avoid contact to any other gas. Electrode 1 was either filled with H_2 or O_2 depending on which battery mode it's working on. Electrode 2 after 1^{st}, 10^{th}, 50^{th}, 100^{th} and 300^{th} cycles were used for characterization such as UV-Vis, FTIR and Raman spectroscopy. For electrically

rechargeable H_2-Q batteries the electrode 1 compartment was filled with H_2 and Q@C as electrode 2. Electrode 2 compartment was purged with an inert gas to avoid contact with other reactive gases. After the discharge, charging is carried out by applying an external bias to the battery.

2.2.1 BATTERY FABRICATION

For Q@C electrode, Q powder and super P of particular composition were grinded well and 10 wt% Nafion® was added along with IPA and sonicated well to get a uniformly dispersed ink. This was coated over toray carbon of 2x2 cm^2 dimension with particular loading. Similarly for Pt@C electrode, sonicated mixer of 40 wt% Pt@C powder, 10 wt% Nafion® and IPA was coated over 2x2 cm^2 toray carbon. Pre-treated Nafion® 212 membrane was sandwiched between these electrodes, such that the catalyst layer facing the membrane to prepare membrane electrode assembly (MEA) (consist of gas diffusion layer (GDL), Pt@C layer, Nafion®, Q@C layer and gas diffusion layer). MEA was then sandwiched between graphite plates with parallel flow fields (figure 2.1), through which gas reach GDL. This was further sandwiched between current collector plates (which helps to connect fuel cell to the external circuit) and end plates (which is used to tighten the system).

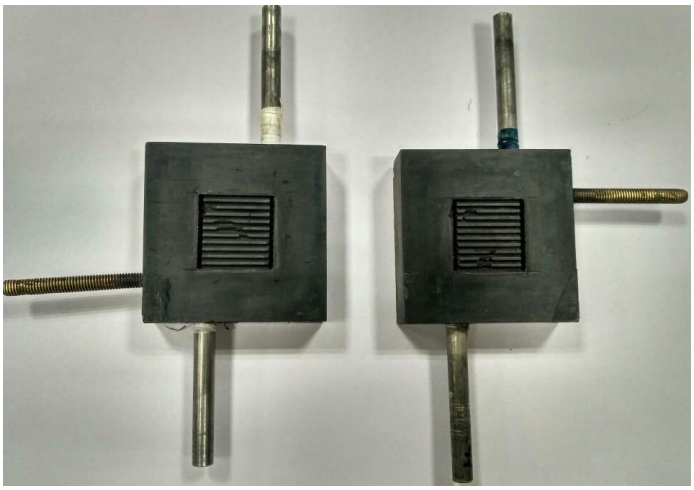

Figure 2.1: Photograph of graphite plates with parallel flow fields

Electrodes used:

Working electrodes: Glassy carbon (0.076, 0.031 cm^2), Platinum mesh electrode, Platinum disc electrode (0.196 cm^2), Platinum disc-Platinum ring electrode.

Reference electrode: Silver-Silver chloride electrode (Ag/AgCl) (E= +0.197 V, 3 M KCl)

Counter electrode: Platinum wire electrode

Table 2.1: Instruments used

Sl no	Instrument	Technique
1	VMP-300 Electrochemical Work Station (Biologics)	Electro chemicals analysis
2	PARSTAT MC (Ametek)	RDE, RRDE
3 4	SEC2000-UV/Vis Spectrometer System, UV-3600 Plus UV-VIS-NIR spectrophotometer	UV-Vis spectroscopy
5	ATR-FTIR (Bruker Alpha FTIR Spectrometer System)	IR spectroscopy
6	LAB-RAM HR 800	Raman spectroscopy

2.3 TECHNIQUES

2.3.1 Electrochemical techniques

2.3.1.1 Cyclic voltammetry (CV)

Cyclic voltammetry is an electrochemical technique, where current is measured while applying a varying potential on the working electrode. Generally done in three electrode system, working electrode (WE) where the electrochemical reaction of analyte in the solution in which it is immersed occur, Counter electrode (CE) helps to complete the circuit, Reference electrode (RE) which helps to sense the potential variation at WE.

Current is measured across WE and CE. Potential is measured across WE and RE. This technique is used to study electrochemical character of analyte in the solution.

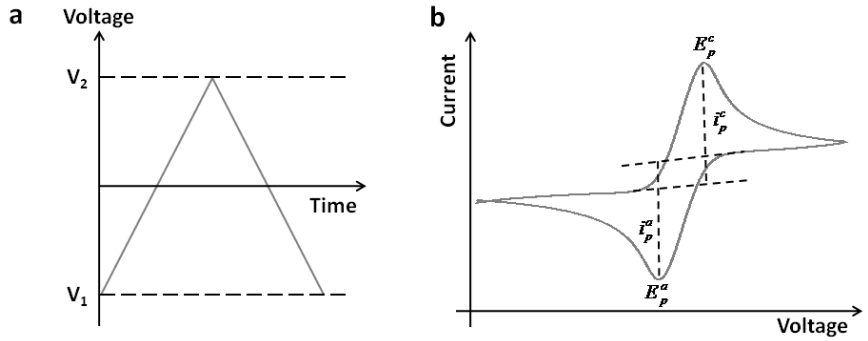

Figure 2.2: (a) The applied voltage on working electrode with respect to time and (b) the current response of this applied voltage. *(http://www.intechopen.com/books/biosensors-for-health-environment-and-biosecurity/biosensors-for-detection-of-low-density-lipoprotein-and-its-modified-forms)*

For reversible system: 1) $i_{pa}/i_{pc} = 1$

2) $E_{pa}-E_{pc} = 0.059/n$ (n - no of electrons)

For non-reversible or quasi reversible: 1) $i_{pa}/i_{pc} \neq 1$

2.3.1.1.1 Randles Sevcik equation: It describes the effect of scan rate on the peak current *I*[24].

$$\boldsymbol{i = 2.68 * 10^5 n^{2/3} A D^{1/2} C \upsilon^{1/2}}$$

i - peak current (A) *n* - number of electrons

A - electrode area (cm^2) *F* - Faraday Constant (96485 C mol^{-1})

D - diffusion coefficient ($cm^2\ s^{-1}$) *C* - concentration (mol cm^{-3})

v - scan rate (V s^{-1}) *R* - Gas constant (J K^{-1} mol^{-1})

T - temperature (K)

i vs. $\upsilon^{1/2}$ plot gives a straight line with slope $2.68 * 10^5 n^{2/3} A D^{1/2} C$, from which unknown parameter can be deduced easily.

***2.3.1.1.2 Cottrell Equation*:** For quasi-reversible and irreversible system Randles sevcik equation given above cannot be used for obtaining parameters like n, A, D, C. The most useful equation in such circumstances is based on of chronoamperometry. The corresponding Cottrell equation describes the current at planar electrodes a function of time following a large over potential as shown below [25].

$$\boldsymbol{i(t) = \frac{nFAD^{1/2}C}{\pi^{1/2}t^{1/2}}}$$

$i(t)$ vs. $t^{-1/2}$ gives a straight line with slope $\frac{nFAD^{1/2}}{\pi^{1/2}t^{1/2}}$, which can be used to deduce various parameters.

i (t) - current (A) n - number of electrons

F - Faraday constant (96485 C mol^{-1}) A - area of the electrode (cm^2)

C - concentration of analyte (mol cm^{-3}) D - diffusion coefficient (cm^2 s^{-1})

t - time (s).

2.3.1.2 Rotating Disc Electrode (RDE) technique

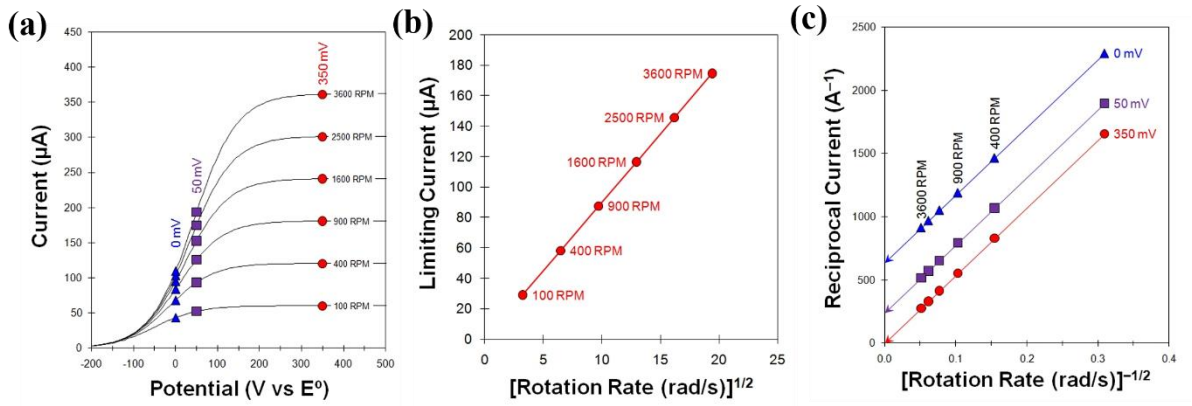

Figure 2.3: (a) RDE linear sweep voltammogram profile for oxidation, (b) Levich plot (c) Koutecky-levich plot.

(https://www.pineresearch.com/shop/knowledgebase/rotating-electrode-theory)

This also done in three electrode system with CE, RE and rotatable WE. CV profile as the one above shows a decrease in current after peak potential. This is due to the diffusion limitation of analyte molecules. This diffusion limitation can be decreased via

using this rotating electrode as working electrode (figure 2.3a). As the electrode rotates hydrodynamic boundary layer is dragged and solution moves away from electrode center due to the centrifugal force. This cause upward perpendicular flow of analyte solution from bulk to replace the boundary layer. This cause the solution to flow towards and across the electrode. The flow rate can be controlled via the rotation rate of electrode. Levich plot and Koutecky-levich plot are used to elucidate parameters from RDE technique[26].

2.3.1.2.1 Levich study: Levich plot with limiting current vs. square root of rotation rate, which gives a straight line with slope of $0.620nFAD^{2/3}v^{-1/6}C$ and intercept zero (figure 2.3b).

$$\boldsymbol{i_L = 0.620nFAD^{2/3}v^{-1/6}C\,\omega^{1/2}}$$

i_L - limiting current — n - no of electrons

F - Faradays constant (96485 C mol^{-1}) — A - area of electrode (cm^2)

D - diffusion coefficient ($cm^2\,s^{-1}$), — υ - kinematic viscosity ($cm^2\,s^{-1}$)

C - concentration (mol cm^{-3}) — ω - rotation rate (rad s^{-1})

2.3.1.2.2 Koutecky-Levich study: In case of kinetic limitations at RDE-electrolyte interface, levich plot alone won't work as it won't be straight. The reciprocal of current (A) vs. reciprocal of square root of rotation rate (rad/sec), which gives a straight line with intercept of reciprocal of i_k (kinetic current) and slope reciprocal of $0.620nFAD^{2/3}v^{-1/6}C$ according to the equation below is called Koutecky-levich plot (figure 2.3c).

$$\boldsymbol{\frac{1}{i} = \frac{1}{i_k} + \frac{1}{i_L}}$$

$$\boldsymbol{\frac{1}{i} = \frac{1}{i_k} + \frac{\omega^{-1/2}}{(0.620nFAD^{2/3}v^{-1/6}C)}}$$

i_L - limiting current — n - no of electrons

F - faradays constant (96485 C mol^{-1}) — A - area of electrode (cm^2)

D - diffusion coefficient ($cm^2\,s^{-1}$), — υ - kinematic viscosity ($cm^2\,s^{-1}$)

C - concentration (mol cm^{-3}) — ω - rotation rate (rad s^{-1})

With this i_k kinetic current we can estimate rate constant of the reaction.

2.3.1.3 Rotating Ring Disc Electrode (RRDE) technique

RRDE is also done in three electrode setup, CE, RE and rotatable WE which have disc in the middle surrounded by a ring. The disc and ring act as two different working electrodes. So the reaction on it can be controlled and monitored with respect to potential we apply[27]. As the product from disc radially move out wards this can be sensed with the ring. RRDE is used to show the reversibility, to find out presence of different type of complex reactions and mechanistic elucidation by detecting transient and short lived reaction intermediates.

2.3.2 UV-Vis spectroscopy

In UV-Vis spectroscopy is used to measure how much light is absorbed or transmitted or reflected by the sample. Wavelength ranging from 190nm to 900nm is used in this technique, generally helps to monitor electronic transitions.

Beer-Lambert-Bouguer law, generally called the Beer-Lambert law suggests that the absorbance (A) is directly proportional to[28]

$$\boldsymbol{A \; \alpha \; Cl}$$

$$\boldsymbol{A \; = \; -log_{10} \left(I_T / I_0\right) \; = \; -\epsilon \; Cl}$$

C - concentration of the sample L - path length

I_0 - intensity on input light I_T - intensity of transmitted light

$\boldsymbol{\epsilon}$ - molar absorption coefficient

2.3.3 Attenuated Total Reflectance (ATR) FT-IR Spectroscopy

IR spectroscopy uses wavelength ranging from 500 cm^{-1} to 4000 cm^{-1}. As vibration frequency of them falls in this range, it helps to identify the functional groups in the molecule. This infrared beam is directed at certain onto an optically dense crystal such as Diamond, Zinc Selenide (ZnSe), Germanium with a high refractive index. An evanescent wave is produce due to this internal reflection. This wave extends beyond the surface of the crystal into the sample held in contact with the crystal. As sample absorbs energy, some region of IR spectrum of evanescent wave would be attenuated. This attenuated energy is passed to IR beam. The IR beam which comes out through the

opposite end is send to the detector which gives us infrared spectrum. As the evanescent wave extends to about 0.5-5 μm from crystal surface, sample should be in close contact with crystal[29].

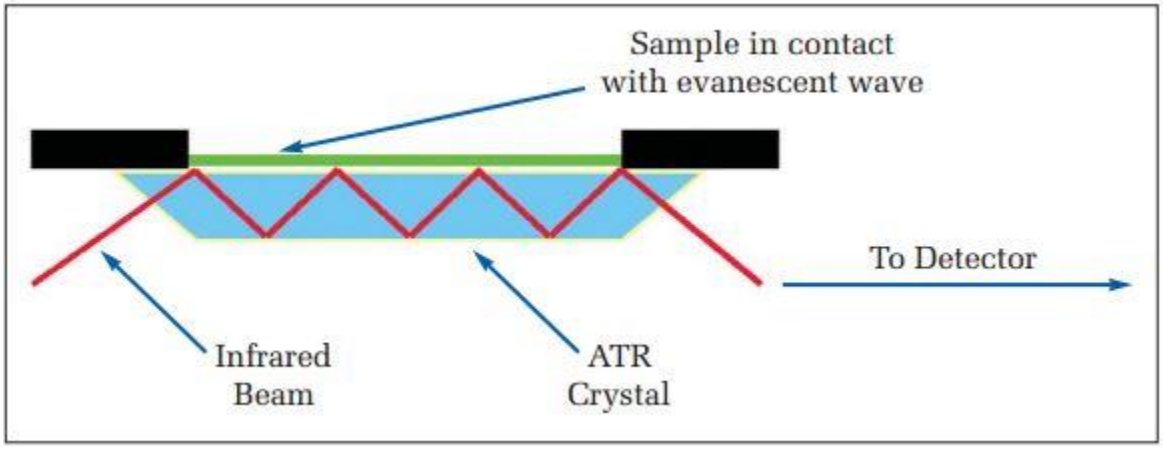

Figure 2.4: Schematic representation of Attenuated Total Reflectance (ATR) IR Spectroscopy *(http://www.utsc.utoronto.ca/~traceslab/ATR_FTIR.pdf)*

2.3.4 Raman spectroscopy

Raman uses the same wavelength range for detection as IR, both gives information about vibrational frequency. IR active vibrational modes needs to have net dipole moment, whereas Raman active once doesn't need net dipole moment.

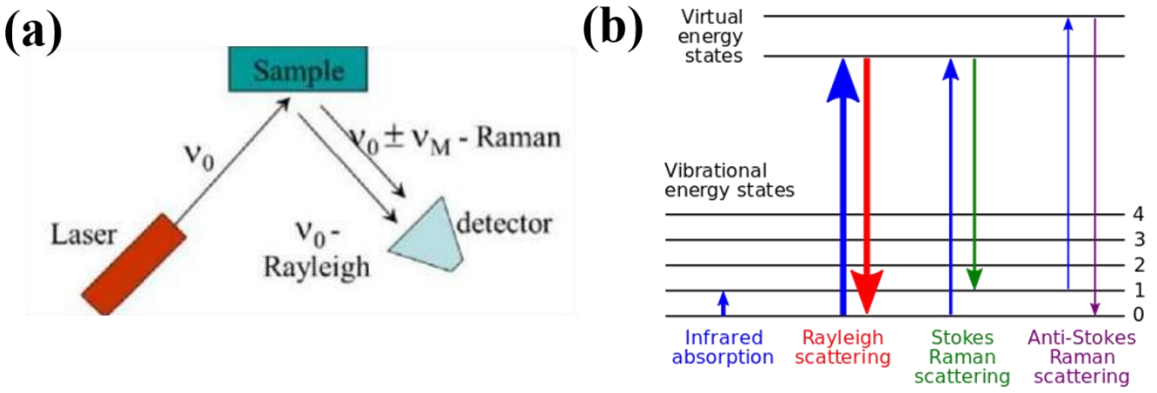

Figure 2.5: (a) Basic principles of Raman analyser. (b) Possible scattering radiations *(http://www.azom.com/article.aspx?ArticleID=10279)* *(http://www.geo.arizona.edu/xtal/geos306/geos306-12.htm)*

Raman spectra is an emission of electromagnetic waves shifted in energy from the incident radiation. Source used in Raman is highly coherent laser source. Laser is focused on the sample, Raman scattered rays reach the detector. Compared to antistokes, stokes shows more intensity, therefore generally stokes is being used for analysis.

CHAPTER 3. RESULTS & DISCUSSION

3.1 INTRODUCTION

Even though the electricity production cost from renewable energy resources have significantly come down, its large scale storage is limited by efficient energy storage modules[30]. Nonetheless energy storage is largely dominated by metal ion batteries and it is well known that state of the art energy storage technologies metal ion have issues related to safety, cost and environmental compatibility [31]. Further they suffer from higher charging voltage than that obtained during the discharge and longer charging time of the order of hours, impeding the much awaited complete electrification of transport. Here we show an air chargeable battery based on H_2, the most abundant element in the universe. The unique feature of this battery is such that it delivers output power during the discharge and air charge process, making it a reversible H^+-ion battery. As the battery can be recharged without an electrical input but with just with air with concomitant power generation even during the charge, we believe this strategy will be a step forward to electrification of transport. Further we extend the concept to construct an electrically chargeable analogue of H^+-ion battery.

3.2 CHEMICALLY CHARGEABLE & REVERSIBLE H^+-ION BATTERY

The proposed battery consists of Pt@C electrode as electrode 1 and a benzoquinone (Q) composite electrode as electrode 2 separated by an H^+-ion conducting Nafion® 212 membrane (Figure 3.1).

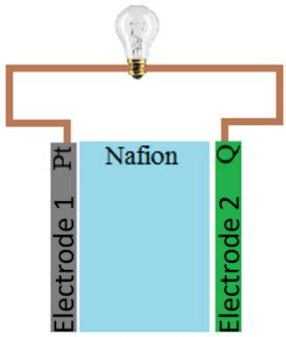

Figure 3.1: Schematic representation of chemically chargeable battery.

We chose benzoquinone as electrode 2 because of its well-known reversible

proton coupled electron transfer, cyclic voltammogram, Figure 3.2a. The plot of equilibrium potential vs. pH (Pourbaix diagram) for the redox transition (Figure 3.2b) is found to be dependent on the pH, demonstrating a slope of -55 mV/pH indicating the electron transfer is accompanied by proton transfer. The square root dependence of the peak current on the scan rate (Figure 3.2c) further indicate a diffusion controlled process which is further clear from the near 1/2 slope of log (i) vs. log (scan rate) plot, Figure 3.2d.

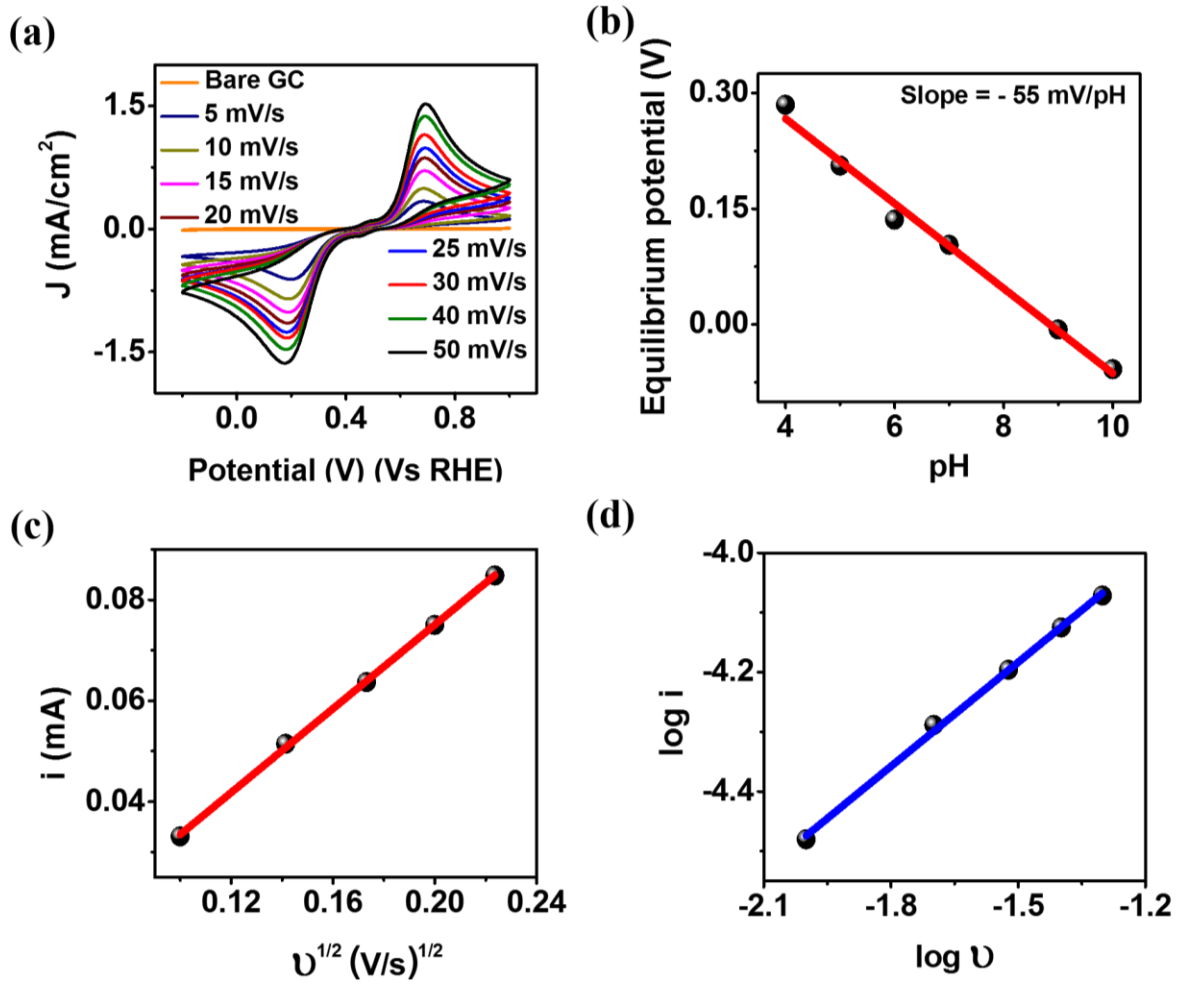

Figure 3.2: (a) Cyclic voltammogram of benzoquinone (Q) in 0.5 M H_2SO_4 on a glassy carbon electrode at different scan rates. It undergoes a reversible and concerted $2e^-$/ $2H^+$ redox reaction to hydroquinone (QH_2) in acidic environment. (b) pH vs. potential (Pourbiax diagram) of 10 mM benzoquinone at different pH demonstrating a negative slope of ~55 mV/pH. (c) Plot of peak current vs. square root of scan rate during the oxidation scan and (d) the corresponding log (i) vs. log (υ) plot.

The diffusion coefficients estimated were estimated from chronoamperometry and the corresponding Cottrell plots (Figures 3.3a and 3.3b). For Q and QH_2 molecules the diffusion coefficients were 5.58×10^{-6} cm^2/s and 6.89×10^{-6} cm^2/s respectively in line with the values reported in literature[32].

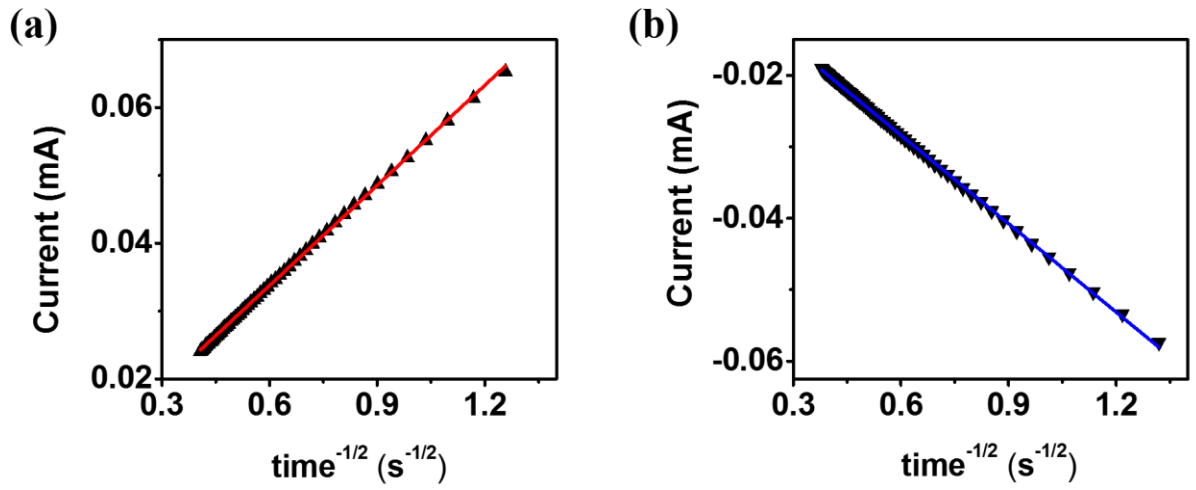

Figure 3.3: Cottrell plots, I vs. reciprocal of square root time (a) for hydroquinone and (b) for benzoquinone.

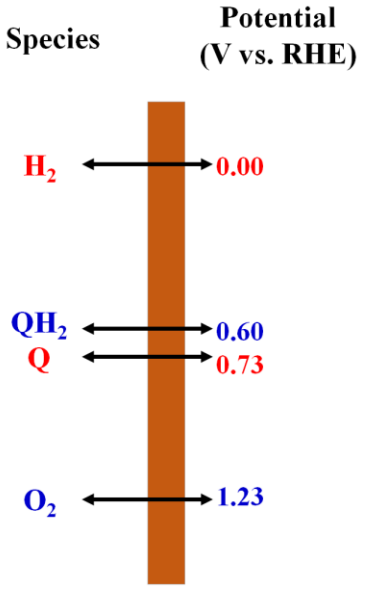

Figure 3.4: Single electrode potentials of Q and QH_2 electrode with respect to H_2/H^+ and O_2/H_2O half-cell reactions. Q is more positive to H_2/H^+ and QH_2 is more negative to O_2/H_2O making the reversible H^+ ion battery feasible.

To understand the electron transfer kinetics of Quinone redox reaction rotating disk electrode (RDE) and rotating ring disk electrode studies (RRDE) were carried out, Figure 3.5. The reversibility of the reaction can be judged from the evident presence of ring currents when the ring is biased at the quinone (Q) reduction potential and the disk is swept towards hydroquinone oxidation potential at a scan rate of 10 mV/s, Figure 3.5a. The Faradaic efficiency of this process at a number of rotations is found to be close to ~100 % indicating decent stability of either redox states under the chosen experimental conditions. The Koutecky-Levich plots (K-L plots), extracted from corresponding LSVs (Figures 3.5b and 3.5c), indicate the number of electrons transferred is close to 2 and the electron transfer rate constant is in the range 10^{-3} cm/s which further indicates a reasonably fast redox reaction, Figure 3.5d, 3.5e and Table 3.1 and 3.2. In essence the redox reactions of quinones are proton coupled and they undergo reasonably fast electron transfer reactions even on simply carbon electrodes and either redox states exhibit decent stability under the chosen experimental conditions.

Table 3.1: Electrochemical parameters extracted from RRDE experiments

Species	No: of electrons	β	Rate constant (cm/s)
Quinone/Hydroquinone	2.06	0.455	$1.3 * 10^{-3}$

Table 3.2: Electrochemical parameters extracted from RDE experiments

E(mV)	Slope	1/Slope	n
600	11495.52	8.69E-05	1.98
625	11225.45	8.90E-05	2.02
650	11164.86	8.95E-05	2.03
675	11152.38	8.96E-05	2.03
700	11145.57	8.97E-05	2.04
725	11154.49	8.96E-05	2.04
750	11171.12	8.95E-05	2.03
800	11183.50	8.94E-05	2.03
990	10943.36	9.13E-05	2.07

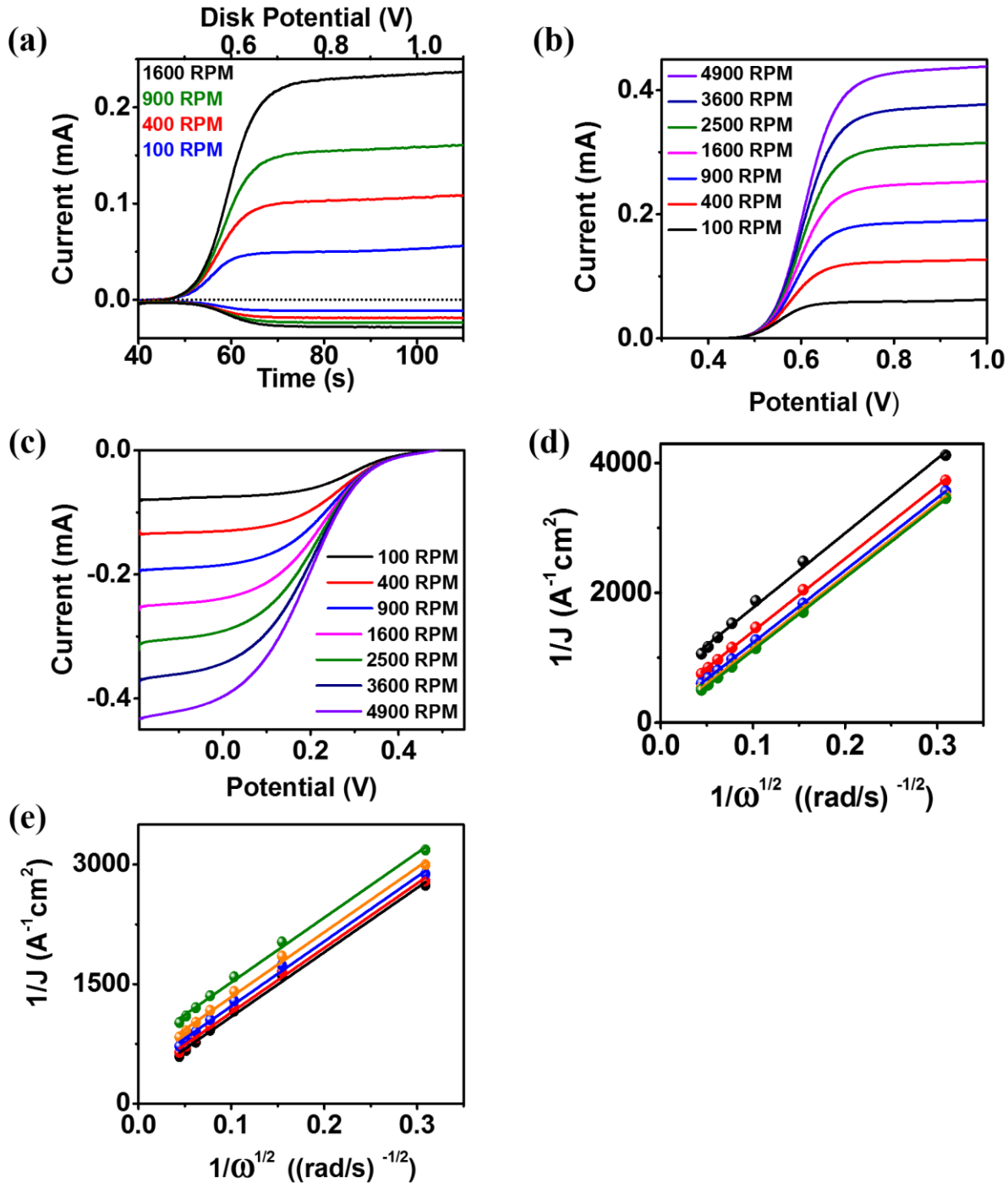

Figure 3.5: (a) RRDE of QH_2 oxidation and reduction at a scan rate of 10 mV/s. Oxidation is carried out potentio-dynamically on the disc and a constant potential of 200 mV reduction potential is applied to the ring at 100-1600 RPM. (b) and (c) RDE of QH_2 oxidation and Q reduction respectively. (d) and (e) Kouteckey-Levich plots for QH_2 oxidation and Q reduction respectively.

To further understand the stability and the nature of the species generated at the electrode/electrolyte interface during the redox reactions of quinones we have carried out UV-Vis spectroelectrochemical studies (Figure 3.6). Very clearly during the oxidation scan the features corresponding to QH_2 disappears (negative going bands) with concomitant appearance of Quinone features (positive bands). On reversing the scan QH_2 bands are restored with gradual disappearance of Quinone features and the original spectrum at the beginning of the scan is restored at the end of reductive potential scan. These indicate reversibility of the reaction and the stability of the corresponding species at the electrode/electrolyte interface.

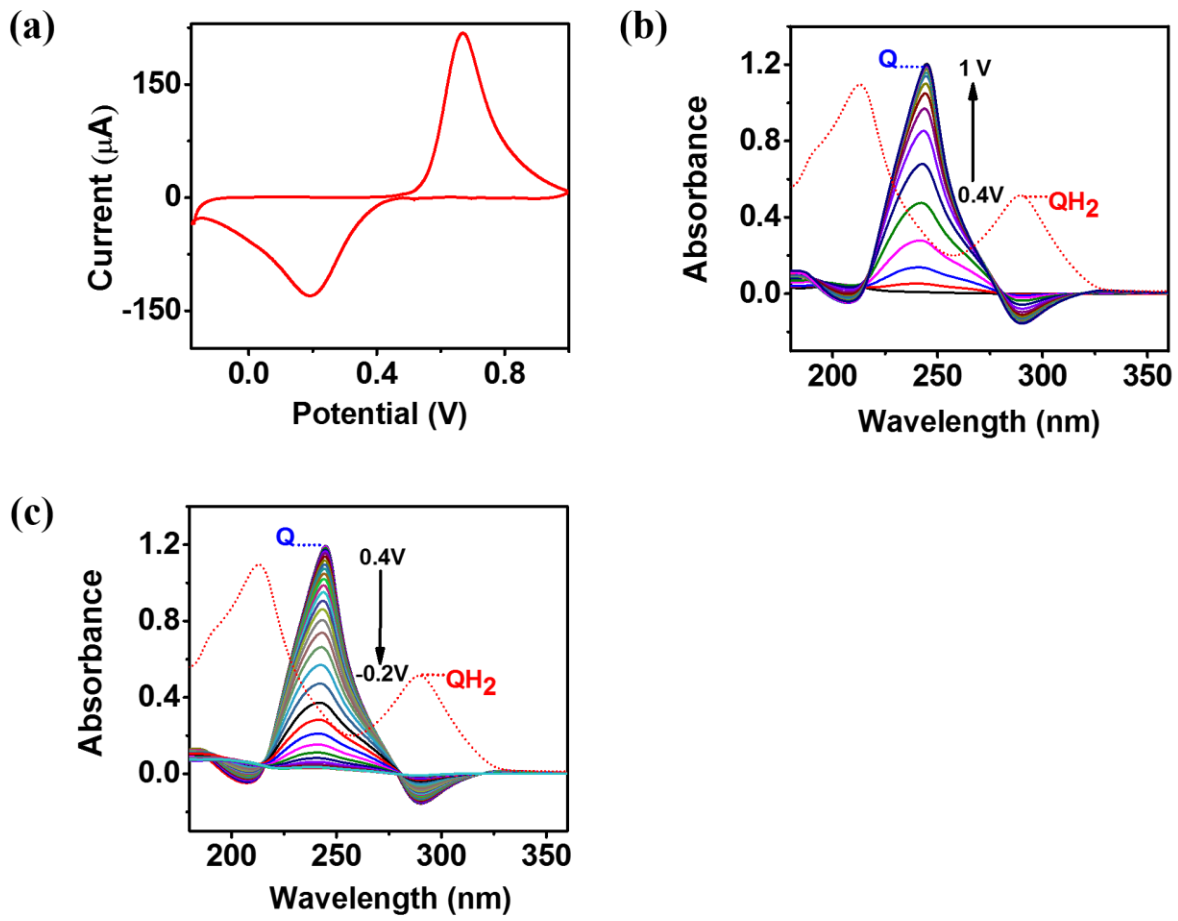

Figure 3.6: In-situ UV-Vis spectroelectrochemistry data for the redox reaction of quinone. (a) Cyclic voltammogram at a scan rate of 5 mV/s. (b) the potential dependent spectra acquired during the oxidation scan and (c) during the reduction scan.

After understanding the electrochemistry of quinones a hydrogen ion battery was fabricated as shown in Figure 3.7. When H_2 is filled into electrode 1 compartment the open circuit voltage between electrode 1 and 2 (battery forward, BF) is found to be ~0.7 V based on the electrode reactions shown in equations 1 and 2 and single electrode potentials, Figure 3.4. Since Pt@C is well known electro-catalyst for H_2 oxidation[18], the generated electrons will move through the external circuit powering the load, and the H^+-ions migrate through the proton exchange membrane to hydrogen acceptor, prompting its conversion to hydroquinone (QH_2), Figure 3.7. At this stage if electrode 1 compartment is fed with O_2, a better hydrogen acceptor than Q, the electron flow will be reversed, and it will be from electrode 2 to electrode 1 (battery reverse, BR) powering the load again with concomitant H^+-ions migration in the opposite direction, equations 3 and 4 and single electrode potentials, Figure 3.4. This is possible mainly because Pt@C is the benchmark electro-catalyst of oxygen reduction reaction[15-17]. The discharge of BR not only produces power but also make the battery ready for next burst of power as it regenerates the Q from QH_2, equations 3 and 4. Therefore H_2 can be fed again to electrode 1 compartment, and power can be obtained between electrode 1 and 2. The above mentioned processes by alternatively filling the electrode compartment 1 with H_2 and O_2 can be repeated several times leading to a sustainable device which can be charged in air with simultaneous power generation.

On passing Hydrogen

Pt@C electrode (anode) $\mathbf{H_2 \rightarrow 2H^+ + 2e^-}$ **…… (1)**

Quinone electrode (cathode) $\mathbf{Q + 2H^+ + 2e^- \rightarrow QH_2}$ **…… (2)**

On passing Oxygen

Quinone electrode (anode) $\mathbf{QH_2 \rightarrow Q + 2H^+ + 2e^-}$ **…… (3)**

Pt@C electrode (cathode) $\mathbf{\frac{1}{2}O_2 + 2H^+ + 2e^- \rightarrow H_2O}$ **…… (4)**

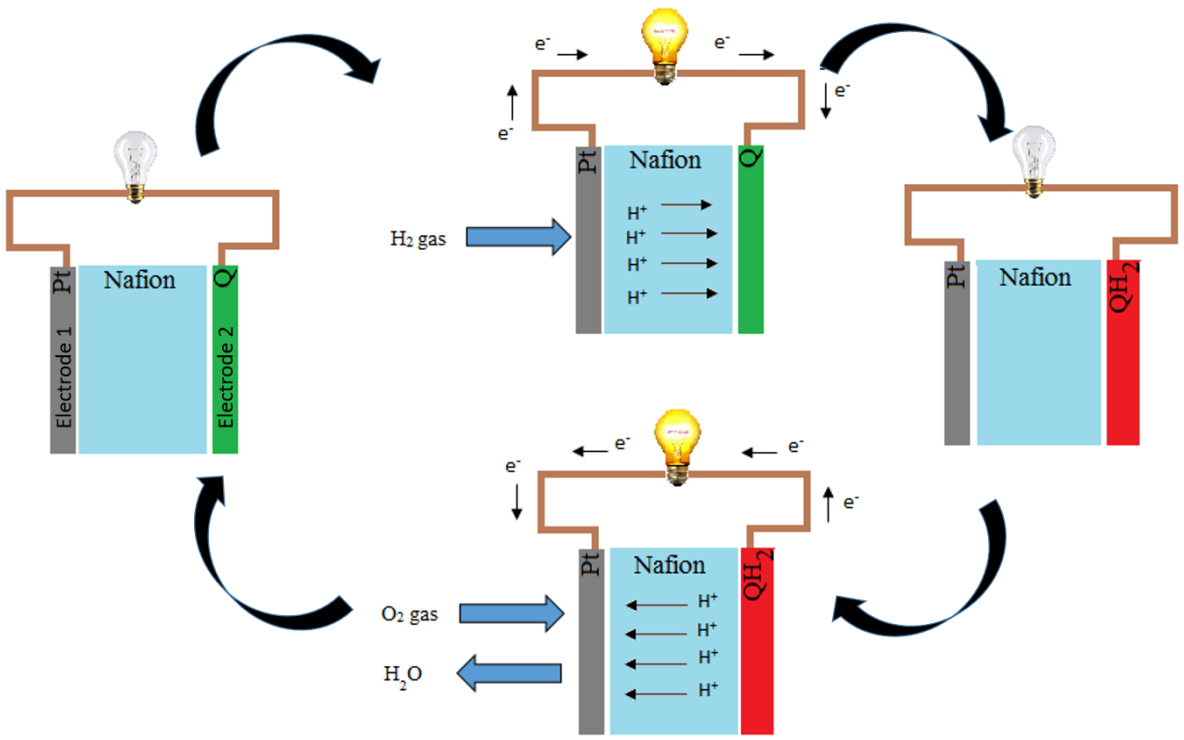

Figure 3.7: Scheme of air chargeable and reversible H^+ ion battery with possible electrode reactions.

In-situ solid state cyclic voltammogram was collected in fuel cell setup, with Pt@C electrode as electrode 1 and benzoquinone electrode as electrode 2. Electrode 2 was always kept in N_2 atmosphere. When Q was the working electrode and on passing H_2 to Pt@C compartment, the redox energy of Q/QH_2 conversion (red line, Figure 3.8a) happened on the positive side suggesting it is an electron acceptor. On the other hand with QH_2 as working electrode, on feeding the Pt@C compartment with O_2, the redox energy of Q/QH_2 occurred in the cathodic regime (blue line, Figure 3.8a) suggesting it is an electron donor. The background voltammogram with N_2 fed to Pt@C compartment demonstrated negligible redox activity, Figure 3.8a black line. These suggest that Q is the cathode for H_2-Q battery and QH_2 is the anode for O_2-QH_2 battery, Figure 3.7. Galvanostatic intermittent titration technique (GITT) was collected for H_2-Q battery to decipher thermodynamic and kinetic parameters. GITT was collected by applying a discharge current of 250 $\mu A/cm^2$ for 5 minutes and then relaxing the system at zero current to open circuit voltage (OCV) for 1 hour. The process is repeated for several hours

to understand phase change and chemical diffusion coefficients. As shown by the blue line in Figure 3.8b, the quasi OCV demonstrated a decline from 600 mV to 480 mV at ~ 25 hours suggesting a clear phase change at the Q electrode. This is in line with the in-situ CV (red line, Figure 3.8a) and the electrode reactions given in equations 1 and 2.

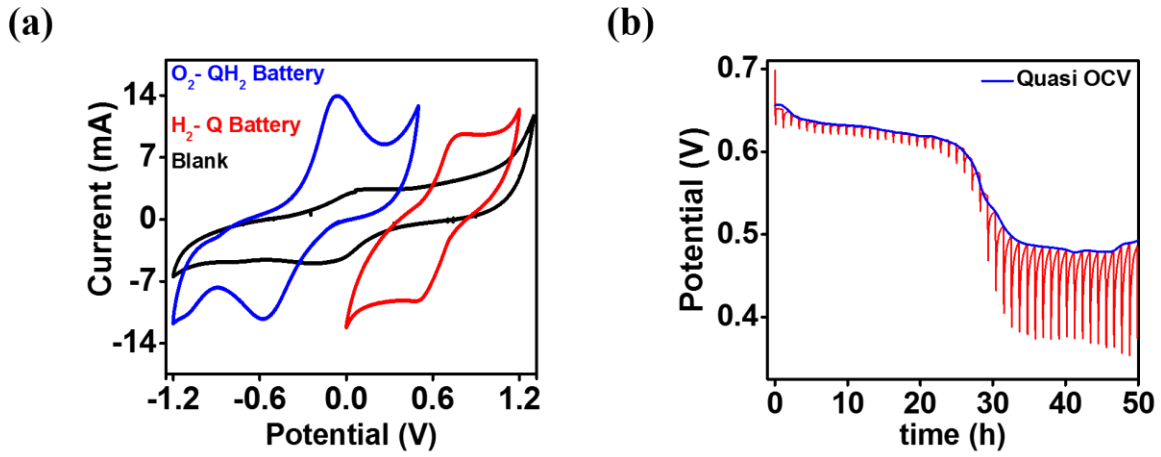

Figure 3.8: (a) In-situ solid state voltammograms of H_2-Q battery (red line) and O_2-QH_2 battery (blue line) along with the background voltammograms in N_2 atmosphere at 5 mV/s scan rate. This suggest that Q is the cathode in H_2-Q battery and QH_2 is the anode in O_2-QH_2 battery. (b) Galvanostatic intermittent titration technique (GITT) data collected for H_2-Q battery. A discharge current of 250 μA/cm^2 was applied for 5 minutes and then the system was relaxed at zero current to open circuit voltage (OCV) for an hour.

The polarization of H_2-Q battery along with the corresponding polarization of O_2-QH_2, Figure 3.9a and 3.9b suggesting the battery can be chemically charged. It should be noted that no external bias is applied to charge the battery after H_2-Q discharge and therefore the O_2-QH_2 charge the H_2-Q battery with concomitant power generation. The H_2-Q demonstrate a power density of 65 mW/cm^2 at a peak current of 170 mA/cm^2 and the maximum current obtained from O_2-QH_2 battery was almost similar to that of H_2-Q battery. The galvanostatic polarization of H_2-Q battery at a rate of 10 mA/cm^2 delivered a discharge capacity of 350 mAh/g (Figure 3.9c) which is 70% of its theoretical discharge capacity, Figure 3.9c. The decrease in discharge capacity from the theoretical value could be due to difficulty of proton diffusion through the ionomer into the composite electrode

and the electronic resistance of the Quinone molecules.

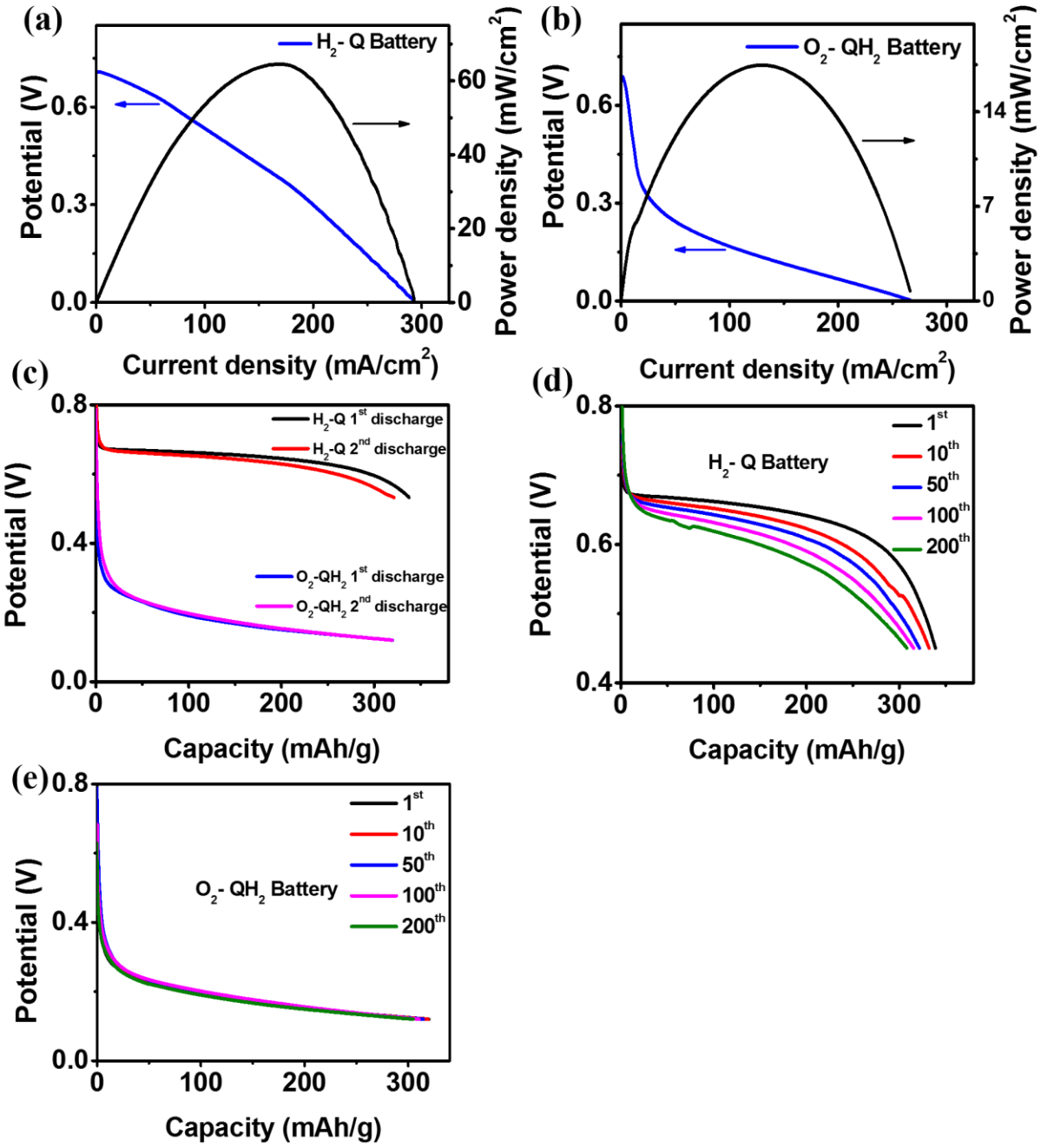

Figure 3.9: (a) Polarization curves for (a) H_2-Q battery and (b) O_2-QH_2 battery. (c) Galvanostatic polarization curves for H_2-Q (10 mA/cm^2) and O_2-QH_2 (5 mA/cm^2) batteries by alternatively filling the Pt@C compartment with H_2 and O_2. (d) Extended cyclability of H_2-Q at 10 mA/cm^2 and (e) O_2-QH_2 batteries at 5 mA/cm^2 by alternatively filling the Pt@C compartment with H_2 and O_2.

Without externally charging the H_2-Q battery, when the Pt@C compartment is fed with O_2, the corresponding discharge delivered approximately the same capacity however with a lower plateau, Figure 3.9c. The lower discharge plateau could be due to the complexity of 4 electron transfer associated with the scission of O_2 molecules compared to H_2[16, 22]. After the O_2-QH_2 discharge when the Pt@C cathode is again filled with H_2, the corresponding H_2-Q battery delivered identical capacity as in the first cycle, Figure 3.9c. This demonstrate that H_2-Q battery can be charged by O_2-QH_2 battery and latter does it with power generation. The discharge of H_2-Q battery further charged the O_2-QH_2 battery and subsequent discharge of O_2-QH_2 furnished identical capacity as in the first cycle, Figure 3.9c. Extended cyclability of the process is given in (Figure 3.9d and 3.9e) for almost 200 cycles, by alternatively filling the Pt@C compartment with H_2 and O_2. It should be noted that there is noticeable capacity decay during cycling and it could be due to sluggish kinetics ORR on Pt@C resulting in incomplete charging. This can be improved modifying the membrane electrode assembly and it will be a matter of future investigations.

To understand the discharge chemistry of the battery the cathode was analyzed by a range of spectroscopic techniques. UV-Vis spectra indicate the transformation of Quinone to QH_2 during the discharge of H_2-Q battery (Figure 3.10a) and reversal of the process during O_2-QH_2 discharge (Figure 3.10b). This indicates the discharge of H_2-Q battery, charge O_2-QH_2 battery and vice versa. Extended cyclability of the discharge processes are shown in Figure 3.10a and 3.10b indicating cyclability over 200 cycles. Discharge processes were further evaluated by FTIR and Raman techniques (Figure 3.10c-3.10f). As shown the discharge of H_2-Q battery generates QH_2, (Figure 3.10c and 3.10e). However during the discharge of O_2-QH_2 battery, the predominant species detected was quinhydrone the charge transfer complex of Quinone and QH_2 (Figure 3.10d and 3.10f). Even though this transformation was visible in the UV-Vis spectra of O_2 charged QH_2 (Figure 3.10b) by the appearance of a broad absorption band in the longer wavelength region, we do not have reason for this transformation at the moment and we believe the higher stability of QH_2 over Q could be driving the formation of charge transfer complexes (Figure 3.11). Extended cyclability of the process is seen in Figure 3.10c-3.10f indicating the sustainability of the process over 200 cycles.

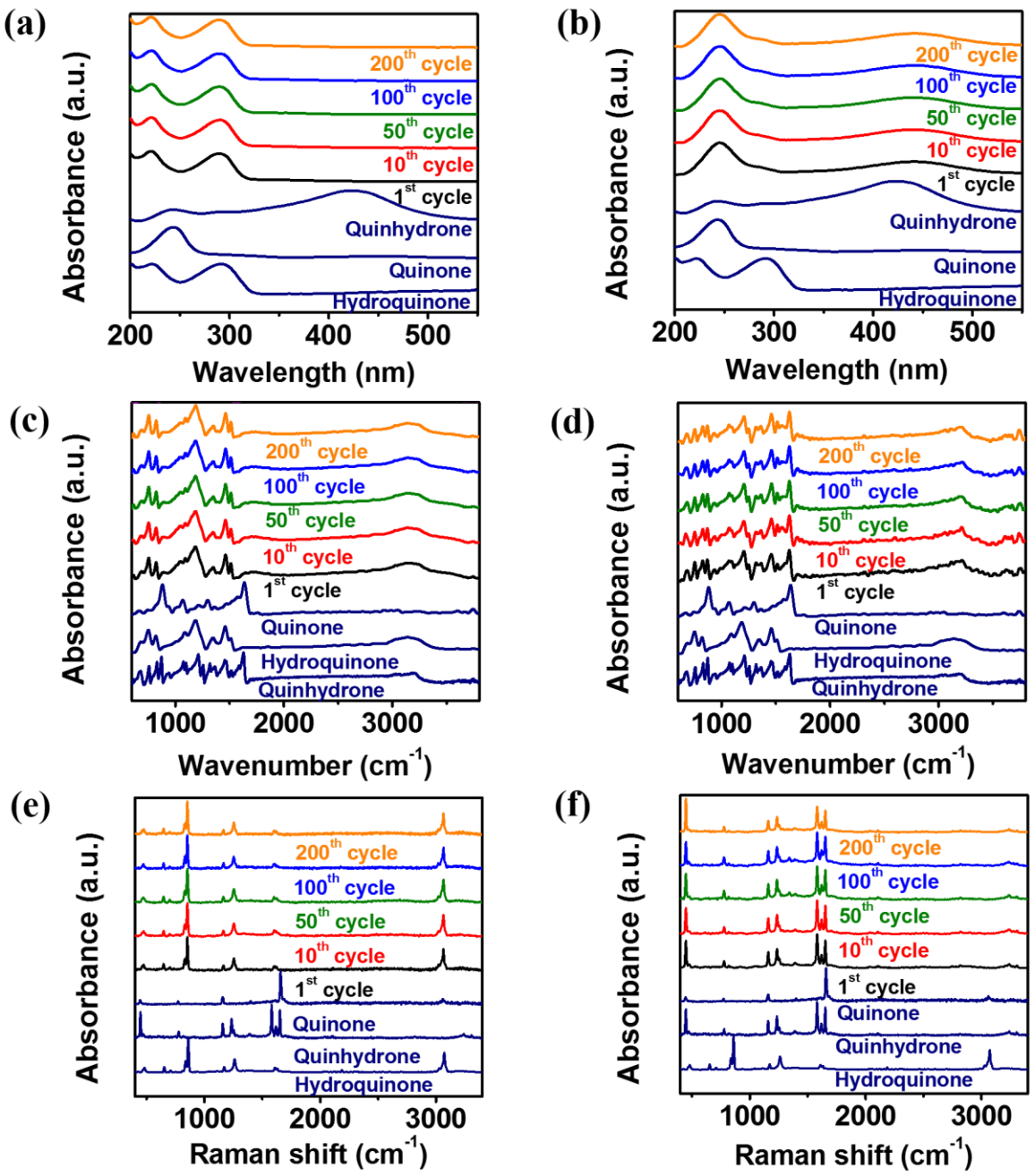

Figure 3.10: UV-Vis spectra of (a) H_2-Q battery cathode and (b) O_2-QH_2 battery anode during different discharge cycles. FTIR spectra of (c) H_2-Q battery cathode and (d) O_2-QH_2 battery anode during different discharge cycles. Raman spectra of (e) H_2-Q battery cathode and (f) O_2-QH_2 battery anode during different discharge cycles.

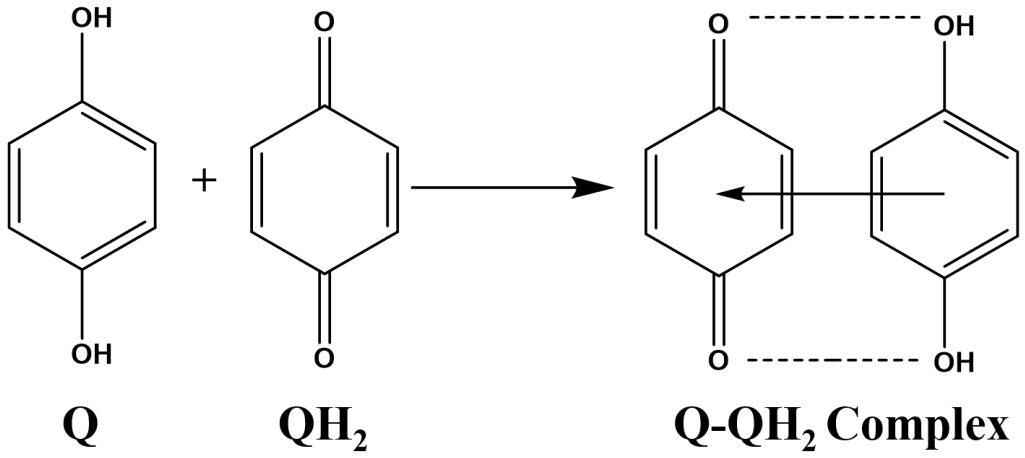

Figure 3.11: Molecular structure of Quinone (Q), Hydroquinone (QH_2) and 1:1 charge transfer complex of Q and QH_2 known as Quinhydrone

3.3 ELECTRICALLY CHARGEABLE H^+-ION BATTERY

H_2-Q battery can be made electrically rechargeable as Q undergoes reversible proton coupled electron transfer, cyclic voltammogram, Figure 3.2a. This is mainly because H_2 evolution can be catalyzed by Pt@C electrode on the anode side during the charge reaction[18, 23]. The polarization curve is shown in Figure 3.9a, demonstrating a remarkable power density of 65 mW/cm^2 at a peak current of 170 mA/cm^2. The battery delivered a discharge capacity of 360 mAh/g at a rate of 10 mA/cm^2, Figure 3.12a. The battery demonstrated decent power capability by delivering 268 mAh/g at a rate of 100 mA/cm^2 and that is 74% of its discharge capacity at 10 mA/cm^2. The rate capability plot during discharge is shown in Figure 3.12b, indicating a polarization below and above the open circuit voltage (OCV) respectively during the discharge and charge chemistries when the rate is gradually increased which is typical of any battery.

Glavanostatic cycling at 50 mA/cm^2 demonstrated cyclability of electrically rechargeable battery and at the end of 300 cycles it retained 88% of its discharge capacity in the first discharge, Figure 3.12c. The voltage efficiency is found to be 64% (Figure 3.12c) which needs to be improved by modifying the electrode structure on the gas diffusion layer. The gap between discharge and charge profiles is almost 290 mV which could be due to the higher electronic resistance of organic electron acceptor (Q/QH_2).

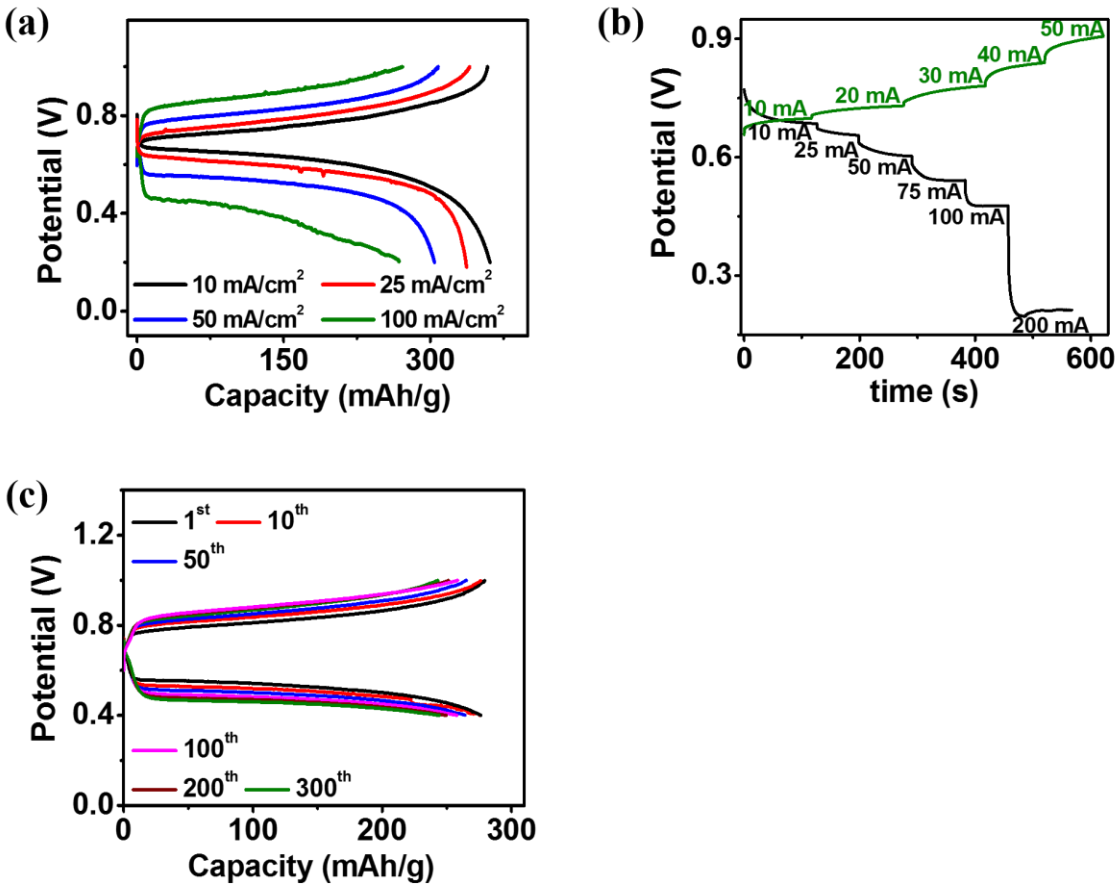

Figure 3.12: (a) Galvanostatic charge discharge curves at different rates for H_2-Q battery. (b) Cell voltage vs. rate plot during discharge and charge chemistries. (c) Galvanostatic cycling at a rate of 50 mA/cm^2 for 300 cycles for H_2-Q battery.

The discharge and charge chemistries are probed by analyzing the cathodes after charge discharge chemistry by various physicochemical techniques. UV-Vis spectroscopy demonstrate the attenuation between Q and QH_2 during discharge chemistry and its reversal during the charge chemistry, Figure 3.13a and 3.13b. The sustainability of the process can be seen over 300 cycles during discharge and charge chemistry. FTIR and Raman spectroscopy further reinforce the formation of QH_2 during discharge chemistry of H_2-Q battery, Figure 3.13c-3.13f. However during the charge chemistry the predominant species identified was quinhydrone as in the case of chemically chargeable Quinone battery explained above. The formation of charge transfer complexes will be a matter of future investigations. In essence an electrochemically

chargeable H_2-Q battery can be constructed and it can be cycled over 300 cycles with decent rate capability and capacity retention.

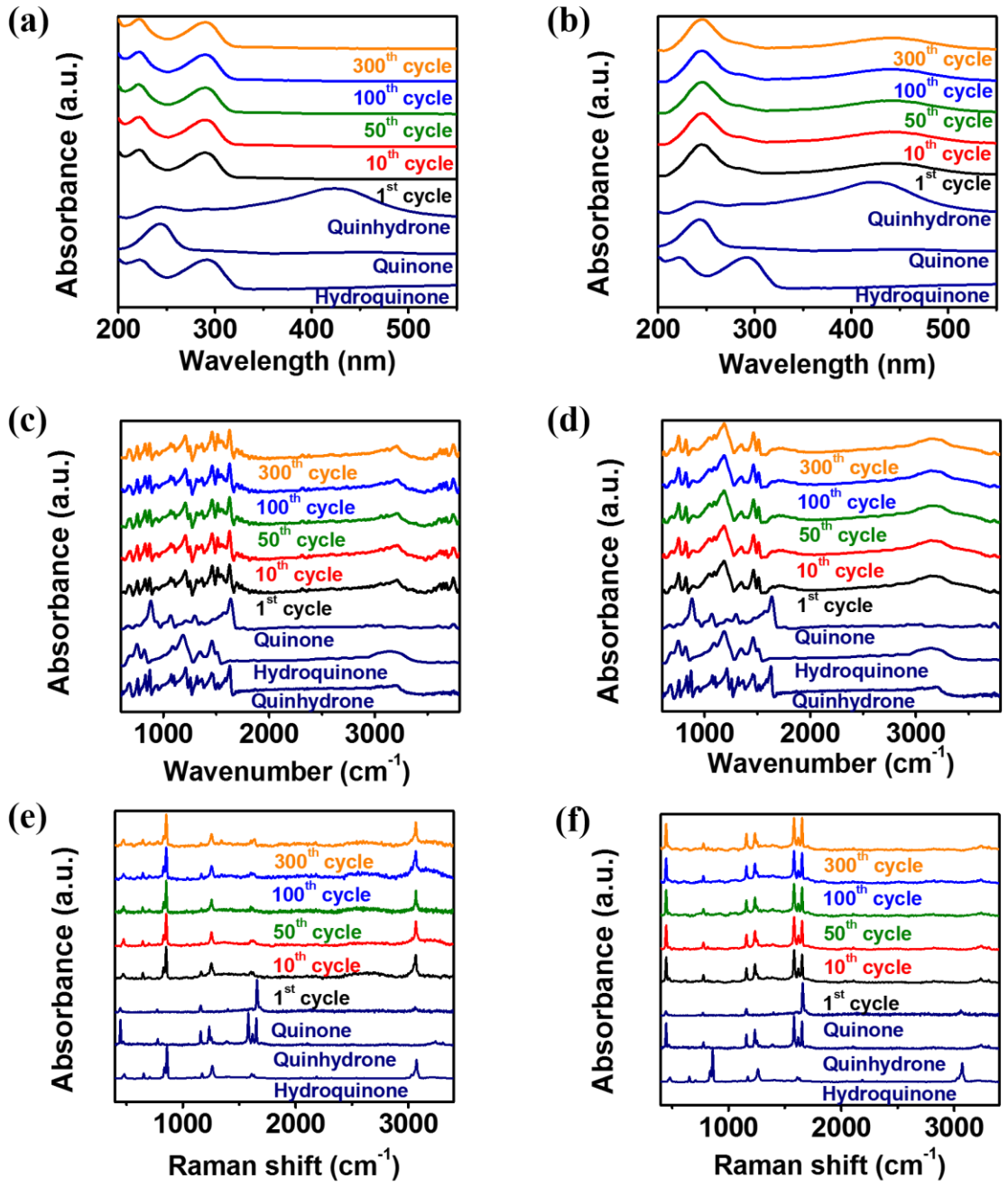

Figure 3.13: UV-Vis spectra of H_2-Q battery cathode (a) during the discharge and (b) during the charge cycles. FTIR spectra of H_2-Q battery cathode (c) during the discharge and (d) during the charge cycles. Raman spectra of H_2-Q battery cathode (e) during the discharge and (f) during the charge cycles.

CHAPTER 4. CONCLUSIONS

The concerted proton coupled electron transfer in Q/QH_2 redox couple can be exploited to construct electrically rechargeable and chemically chargeable H^+ ion battery. Their charge discharge chemistries were investigated. It is found that the redox energy of Q favors electron acceptance when the electrocatalytic compartment is filled with H_2. On filling the catalytic chamber with O_2, discharged QH_2 behaves as an electron donor ultimately leading to a reversible and air chargeable H^+ ion battery. It should be noted that this battery produces an output power during discharge and chemical charge processes with extended cyclability over 200 cycles. The catalytic nature of Pt@C electrode for H_2 evolution could be further exploited for designing an electrically chargeable analogue of H^+ ion battery. UV-Vis, RRDE, GITT, FTIR and Raman spectroscopy techniques were adopted to elucidate the discharge and charge chemistries and it evidence the formation of QH_2 during discharge and predominantly quinhydrone during the charge chemistries. The generation of charge transfer complexes are a matter of future investigations. Future efforts will be dedicated to improve voltage efficiency, columbic efficiency and overall energy efficiency of electrically chargeable and chemically chargeable batteries.

REFERENCES

1. Bruce, P. G., Freunberger, S. A., Hardwick, L. J. & Tarascon, J. M. Li–O_2 and Li–S batteries with high energy storage. *Nat. Mater*. **2012**, *11*, 19–29.
2. Robert C. Armstrong, Catherine Wolfram, Krijn P. de Jong, Robert Gross, Nathan S. Lewis, Brenda Boardman, Arthur J. Ragauskas, Karen Ehrhardt-Martinez, George Crabtree & M. V. Ramana, The frontiers of energy, *Nature Energy*, **2016**, *1*
3. Steven Chu, Yi Cui & Nian Liu, The path towards sustainable energy *Nature Materials*, **2017**, *16*, 16–22
4. Chu, Steven, and Arun Majumdar., Opportunities and challenges for a sustainable energy future, *Nature*, **2012**, *488*, 294-303.
5. Bruno Scrosati, Jusef Hassoun and Yang-Kook Sun, Lithium-ion batteries. A look into the future*, Energy Environ. Sci.*, **2011**, *4*, 3287-3295
6. Alain Goeppert, Miklos Czaun, G. K. Surya Prakash and George A. Olah, Air as the renewable carbon source of the future: an overview of CO_2 capture from the atmosphere, *Energy Environ. Sci.*, **2012**, *5*, 7833-7853
7. Philippe Poizot and Franck Dolhem, Clean energy new deal for a sustainable world: from non-CO_2 generating energy sources to greener electrochemical storage devices, *Energy Environ. Sci*., 2011, *4*, 2003-2019.
8. Mark Z. Jacobson**,** Review of solutions to global warming, air pollution, and energy security, *Energy Environ. Sci*., **2009**, *2*, 148-173
9. Grätzel, M. Photovoltaic and photo electrochemical conversion of solar energy. Philosophical Transactions. Series A, Mathematical, Physical, and Engineering Sciences. **2007**, *365*, 993–1005
10. Martin Winter, Ralph J. Brodd, What Are Batteries, Fuel Cells, and Supercapacitors?, *Chem. Rev*. **2004**, *104*, 4245-4269
11. Kristy Jost, Genevieve Dion and Yury Gogotsi, Textile energy storage in perspective, *J. Mater. Chem. A,* **2014**, ***2***, 10776-10787
12. M. Rosa Palacín, Recent advances in rechargeable battery materials: A chemist's perspective, *Chem. Soc. Rev*., **2009,** *38*, 2565-2575

13. Jaime Wisniak, Electrochemistry and Fuel Cells: The Contribution of William Robert Grove*, Indian Journal of History of Science*, **2015**, *50*, 476-490
14. Marvin Warshay, Paul R. Prokopius, The fuel cell in space: yesterday, today and tomorrow, *Journal of Power Sources*, **1990**, *29*, 193-200
15. Markus Nesselberger, Melanie Roefzaad, R. Fayçal Hamou, P. Ulrich Biedermann, Florian F. Schweinberger, Sebastian Kunz, Katrin Schloegl, Gustav K. H. Wiberg, Sean Ashton, Ueli Heiz, Karl J. J. Mayrhofer & Matthias Arenz, The effect of particle proximity on the oxygen reduction rate of size-selected platinum clusters*, Nature Materials*, **2013**, *12*, 919–924
16. Jinho Park, Lei Zhang, Sang-Il Choi, Luke T. Roling , Jeffrey A. Herron, Shuifen Xie, Jinguo Wang, Moon J. Kim, Manos Mavrikakis, and Younan Xia. Atomic layer-by-layer deposition of platinum on palladium octahedra for enhanced catalysts toward the oxygen reduction reaction, *ACS Nano*, **2015**, *9*, 2635–2647
17. Hubert A. Gasteiger, Shyam S. Kocha, Bhaskar Sompalli, Frederick T. Wagner, Activity benchmarks and requirements for Pt, Pt-alloy, and non-Pt oxygen reduction catalysts for PEMFCs*, Applied Catalysis B: Environmental*, **2005**, *56*, 9–35
18. Tran N. Huan, Reuben T. Jane, Anass Benayad, Laure Guetaz, Phong D.Tran and Vincent Artero, Bio-inspired noble metal-free nanomaterials approaching platinum performances for H_2 evolution and uptake, *Energy Environ. Sci.*, **2016**, *9*, 940-947
19. Michael G. Walter, Emily L. Warren, James R. McKone, Shannon W. Boettcher, Qixi Mi, Elizabeth A. Santori, and Nathan S. Lewis, Solar Water Splitting Cells, *Chem. Rev*. **2010**, *110*, 6446–6473
20. Mark K. Debe, Electrocatalyst approaches and challenges for automotive fuel cells, *Nature*, **2012**, *486*, 43-51
21. S. Litster, G. McLean, PEM fuel cell electrodes, *J. of Power Sources*, **2004**, *130*, 61-76
22. Oliver T. Holton and Joseph W. Stevenson, The Role of Platinum in Proton Exchange Membrane Fuel Cells*, Platinum Metals Rev*., **2013**, *57*, 259–271
23. Huajie Yin, Shenlong Zhao, Kun Zhao, Abdul Muqsit, Hongjie Tang,Lin Chang, Huijun Zhao, Yan Gao & Zhiyong Tang, Ultrathin platinum nanowires grown on single-

layered nickel hydroxide with high hydrogen evolution activity*, Nature Communications*, **2015**, *6*, 6430

24. A. J. Bard and L. R. Faulkner, *Electrochemical Methods: Fundamental and Applications*, John Wiley, New York, **2001**
25. A.J. Bard, L.R. Faulkner, *Electrochemical Methods, Fundamentals and Applications*, Wiley, New York, **1980**
26. Shun Mao, Zhenhai Wen, Taizhong Huang, Yang Houa, Junhong Chen, High-performance bi-functional electrocatalysts of 3D crumpled graphene–cobalt oxide nanohybrids for oxygen reduction and evolution reactions, *Energy Environ. Sci.*, **2014**, *7*, 609
27. Stephen Treimer, Andrew Tanga , and Dennis C. Johnson, Review A Consideration of the Application of Koutecky¬-Levich Plots in the Diagnoses of Charge-Transfer Mechanisms at Rotated Disk Electrodes*, Electroanalysis*, **2002**, *14*, 165-171
28. C. N. Banwell, E. M. McCash, A Book: *Fundamentals of Molecular Spectroscopy,* 4th Ed. Tata McGraw Hill Publishing Co. Ltd., **2002**
29. Ramer, G. and Lendl, B, *Attenuated Total Reflection Fourier Transform Infrared Spectroscopy. Encyclopedia of Analytical Chemistry. (ATR)*. **2013**
30. Bruce Dunn, Haresh Kamath, Jean-Marie Tarascon, Electrical energy storage for the grid: A battery of choices, *Science* , **2011**, *334*, 928-935
31. Hu-Rong Yao, Ya You, Ya-Xia Yin, Li-Jun Wan and Yu-Guo Guo*,* Rechargeable dual-metal-ion batteries for advanced energy storage, *Physical Chemistry Chemical Physics*, **2016**, ***18***, 9326-9333
32. William M. Flarsheim, Yu-Min TSOU, Isaac Trachtenberg, Keith P. Johnston: and Allen J. Bard**,** Electrochemistry in near-critical and supercritical fluids. 3. Studies of bromide, iodide and hydroquinone in aqueous solutions, *J. Phys. Chem.,* **1986**, *90,* 3857-3862